



**HAL**  
open science

# Assessing the performance of adsorbents for CO<sub>2</sub>/CH<sub>4</sub> separation in pressure swing adsorption units: A review

Luis Paz, Solène Gentil, Vanessa Fierro, Alain Celzard

## ► To cite this version:

Luis Paz, Solène Gentil, Vanessa Fierro, Alain Celzard. Assessing the performance of adsorbents for CO<sub>2</sub>/CH<sub>4</sub> separation in pressure swing adsorption units: A review. *Journal of Environmental Chemical Engineering*, 2024, 12 (6), pp.114870. 10.1016/j.jece.2024.114870 . hal-04960059

**HAL Id: hal-04960059**

<https://hal.univ-lorraine.fr/hal-04960059v1>

Submitted on 21 Feb 2025

**HAL** is a multi-disciplinary open access archive for the deposit and dissemination of scientific research documents, whether they are published or not. The documents may come from teaching and research institutions in France or abroad, or from public or private research centers.

L'archive ouverte pluridisciplinaire **HAL**, est destinée au dépôt et à la diffusion de documents scientifiques de niveau recherche, publiés ou non, émanant des établissements d'enseignement et de recherche français ou étrangers, des laboratoires publics ou privés.



Distributed under a Creative Commons Attribution 4.0 International License

1  
2  
3  
4  
5  
6  
7  
8  
9  
10  
11  
12  
13  
14  
15  
16  
17  
18  
19  
20  
21  
22  
23

# Assessing the Performance of Adsorbents for CO<sub>2</sub>/CH<sub>4</sub> Separation in Pressure Swing Adsorption units: a Review

Luis Paz<sup>a</sup>, Solène Gentil<sup>b</sup>, Vanessa Fierro<sup>a,\*</sup> and Alain Celzard<sup>a,c,\*</sup>

<sup>a</sup> *Université de Lorraine, CNRS, IJL, Epinal, F-88000, France*

<sup>b</sup> *Groupe BORDET, Froidvent, F-21290 Leuglay, France*

<sup>c</sup> *Institut Universitaire de France (IUF), F-75231 Paris, France.*

---

\* Corresponding authors: Alain Celzard ([alain.celzard@univ-lorraine.fr](mailto:alain.celzard@univ-lorraine.fr)), Vanessa Fierro ([vanessa.fierro@univ-lorraine.fr](mailto:vanessa.fierro@univ-lorraine.fr)), Université de Lorraine.

## 24 **Assessing the Performance of Adsorbents for CO<sub>2</sub>/CH<sub>4</sub> Separation in** 25 **Pressure Swing Adsorption Units: a Review**

26 This review article assesses the performance of various adsorbents for CO<sub>2</sub>/CH<sub>4</sub>  
27 separation, a critical step in the final phase of a biogas upgrading plant. The focus  
28 is particularly on the use of pressure swing adsorption (PSA) units for this  
29 purpose. Four types of adsorbents, including activated carbons (ACs), carbon  
30 molecular sieves, metal organic frameworks, and zeolites, are thus evaluated  
31 based on their selectivity in CO<sub>2</sub>/CH<sub>4</sub> separation and PSA working capacity ratio.  
32 This selectivity is estimated from pure component isotherms through the Ideal  
33 Adsorbed Solution Theory (IAST), and the PSA working capacity ratio is  
34 evaluated for a PSA cycle with depressurization at atmospheric and sub-  
35 atmospheric pressure. The results show that ACs exhibit the lowest selectivity,  
36 while zeolites have the highest selectivity and PSA working capacity ratio. The  
37 article also includes a review of simulation studies on CO<sub>2</sub>/CH<sub>4</sub> separation by  
38 PSA. In addition, PSA units are compared based on their productivity, energy  
39 consumption, purity, and recovery. To calculate energy consumption and  
40 productivity, parameters that are often overlooked, a mass balance is applied to  
41 the PSA cycle described in each relevant literature study. Our study suggests that  
42 the PSA cycle with pressure equalization and sub-atmospheric pressure  
43 depressurization is the most optimal, providing valuable insights into the  
44 selection and optimization of adsorbents and PSA units for CO<sub>2</sub>/CH<sub>4</sub> separation.

45 **Keywords:** biogas upgrading; CO<sub>2</sub>/CH<sub>4</sub> separation; adsorption; pressure swing  
46 adsorption units.

47

48

49

50

51

52

53

54

## 55 **1. Introduction**

56 Biogas, a byproduct of the anaerobic decomposition of organic matter, represents a  
57 promising strategy for reducing greenhouse gas (GHG) emissions. It primarily  
58 comprises methane ( $\text{CH}_4$ ) and carbon dioxide ( $\text{CO}_2$ ), but can also contain several other  
59 impurities, including  $\text{H}_2\text{S}$ ,  $\text{NH}_3$ , water vapor,  $\text{N}_2$ ,  $\text{H}_2$ ,  $\text{CO}$ ,  $\text{O}_2$ , and siloxanes.<sup>[1]</sup> These  
60 constituents, although present in significantly lower proportions than  $\text{CH}_4$  and  $\text{CO}_2$ , can  
61 exert a notable detrimental influence on the final utility of biogas. When upgrading  
62 biogas for increased  $\text{CH}_4$  purity, the initial focus is typically on eliminating  $\text{H}_2\text{S}$ , given  
63 its potential corrosive threat and the need to protect treatment facilities. Subsequently,  
64 additional treatment is applied to remove the remaining contaminants in order to obtain  
65 a biogas primarily comprising  $\text{CH}_4$  and  $\text{CO}_2$ .

66 Among the methods available to perform  $\text{CH}_4/\text{CO}_2$  separation, pressure swing  
67 adsorption (PSA), which uses adsorbent materials, is gaining in popularity due to its  
68 energy efficiency, low operating and installation costs, compact equipment design and  
69 user-friendly operation.<sup>[2]</sup>  $\text{CO}_2$  adsorption has mainly been studied using activated  
70 carbons (ACs), carbon molecular sieves (CMSs), zeolites and metal-organic  
71 frameworks (MOFs). Despite extensive investigation, many adsorbents exhibit limited  
72 adsorption capacity or are expensive to produce. Addressing these challenges requires  
73 the development of porous materials that are both cost-effective and easy to regenerate,  
74 and offer high adsorption capacity and selectivity.<sup>[3]</sup>

75 The aim of this study is to identify the most effective adsorbent materials and PSA  
76 systems for separating  $\text{CO}_2$  from  $\text{CH}_4$ . Unlike previous studies that focused on  
77 comparing the physicochemical properties,  $\text{CO}_2$  and  $\text{CH}_4$  uptake, and  $\text{CO}_2/\text{CH}_4$   
78 selectivity of various adsorbents using manometric equipment at laboratory scale,<sup>[4, 5]</sup>  
79 this work examines the performance of selected adsorbents tested in PSA conditions.

80 For that purpose, we consider a fundamental operational parameter in PSA systems,  
81 adsorption pressure, which is the pressure at which adsorption occurs in the PSA  
82 column containing the adsorbent material. Since operating pressure depends on the  
83 specific PSA regeneration method, our investigation centers on two distinct adsorption  
84 pressures: 5 bar, which is generally the operating pressure for systems undergoing  
85 depressurization to atmospheric levels, and 1 bar, representative of the average  
86 operating pressure for systems using depressurization to sub-atmospheric levels.

87 In the present study, we use the pure CO<sub>2</sub> and CH<sub>4</sub> adsorption isotherms to conduct  
88 simulations and predict their co-adsorption when mixed by employing the IAST (Ideal  
89 Adsorbed Solution Theory) method. Then, the estimated amounts of CO<sub>2</sub> and CH<sub>4</sub>  
90 adsorbed from the gas mixture are used to calculate the equilibrium selectivity and PSA  
91 working capacity ratio for each adsorption operating pressure. While existing review  
92 articles have already explored the performance of PSA systems for CO<sub>2</sub>/CH<sub>4</sub> separation  
93 under various operating conditions,<sup>[6-10]</sup> our approach transcends the limitations of  
94 reported data. We employ full mass balances considering flow rates for the inlet, outlet,  
95 purge and vent stages. This approach allows us to calculate the CH<sub>4</sub> productivity and the  
96 expected energy consumption of the PSA. These two factors are indeed key  
97 performance indicators (KPIs) often overlooked by researchers who concentrate solely  
98 on assessing the final purity and recovery from the PSA. In this review paper, we will  
99 demonstrate that considering these two KPIs, it is possible to select the most optimal  
100 operating mode in PSA units.

101

## 102 2. Generalities on Biogas Production

### 103 2.1 Typical Composition and Applications of Biogas

104 Fossil fuels currently account for over 75% of the world's total energy supply<sup>[11]</sup> and  
105 are the primary source of GHG emissions, the cause of global warming. In order to meet  
106 the European Union's (EU) objective of reducing GHG emissions by at least 55% by  
107 2030 and achieving net zero emissions by 2050,<sup>[12]</sup> the use of biomethane emerges as a  
108 promising strategy. Moreover, the EU is currently facing geopolitical challenges  
109 associated with natural gas imports, and is striving to reduce its dependence on external  
110 suppliers. This underscores the importance of biomethane production, which is  
111 anticipated to witness a substantial increase, as shown in **Figure 1**.

112 **[Figure 1 here]**

113 Biomethane is mainly obtained from biogas, from which it needs to be separated.  
114 Biogas is a byproduct of the anaerobic decomposition of organic matter, including  
115 animal manure, plant debris, food waste, biodegradable parts of municipal waste and  
116 sewage sludge. The precise composition of biogas depends on the source of the organic  
117 matter undergoing decomposition, as shown in **Table 1**.

118 **[Table 1 here]**

119 Since CO<sub>2</sub> can account for up to 50 vol.% of biogas composition, and is not  
120 combustible, this compound significantly reduces the high heating value (HHV) of  
121 biogas (21.5 MJ·Nm<sup>-3</sup>) compared with natural gas (39.8 MJ·Nm<sup>-3</sup>),<sup>[13]</sup> which is mainly  
122 composed of methane. Upgrading biogas can improve its HHV by up to 30 MJ·Nm<sup>-3</sup>.<sup>[6]</sup>  
123 Additionally, CO<sub>2</sub> hinders biogas compression, a process commonly employed for its  
124 storage.<sup>[14]</sup>

125 Other impurities, such as hydrogen sulfide ( $\text{H}_2\text{S}$ ) or ammonia ( $\text{NH}_3$ ), can have  
126 various adverse effects.  $\text{H}_2\text{S}$ , for instance, is known for its corrosive impact on internal  
127 combustion engines, and it can present serious risks to human health. On the other hand,  
128 the accumulation of  $\text{NH}_3$  is a potential issue in the anaerobic digestion of food waste,<sup>[15]</sup>  
129 restricting its application in industrial biogas plants. Since a high concentration of  $\text{NH}_3$   
130 can lead to a 50% reduction in  $\text{CH}_4$  production,<sup>[15]</sup>  $\text{NH}_3$  is normally treated in the  
131 anaerobic digester using nitrification/denitrification techniques.

132 Siloxanes are a common impurity, particularly when biogas is produced from sources  
133 such as landfills. When siloxane-containing biogas is burned in an engine, the siloxanes  
134 undergo oxidation to form silicon dioxide, which can accumulate on engine components  
135 such as spark plugs, valves and turbo compressors.<sup>[16]</sup> Finally, the presence of moisture  
136 can adversely affect the  $\text{CO}_2$  adsorption process on zeolites and MOFs during biogas  
137 upgrading. However, the influence of moisture on carbon surfaces remains a matter of  
138 debate, as it has been shown to even improve  $\text{CO}_2$  adsorption compared to dry  
139 conditions.<sup>[17]</sup> Nevertheless, it is crucial to recognize a threshold beyond which the  
140 presence of water can exert a negative effect on  $\text{CO}_2$  adsorption. Studies indicate that  
141 when the water content exceeds 1 vol.%,<sup>[18]</sup> or relative humidity exceeds 37% in the gas  
142 phase,<sup>[19]</sup>  $\text{CO}_2$  adsorption drops substantially.

143 When biogas is upgraded to a higher  $\text{CH}_4$  purity, it is referred to as “renewable  
144 natural gas” or “biomethane ( $\text{Bio-CH}_4$ )” and can be used in a variety of power  
145 generation applications, including heat, electricity and fuel, as shown in **Figure 2**. A  
146 more detailed comparison of biogas applications can be found elsewhere.<sup>[20, 21]</sup> Overall,  
147 the conversion of biogas into  $\text{Bio-CH}_4$  emerges as a promising route for the production  
148 and transportation of sustainable energy, offering a viable alternative to fossil fuels.

149 **[Figure 2 here]**

## 150 **2.2 Biogas Upgrading**

151 Several methods can be used to upgrade biogas,<sup>[22]</sup> and the choice of the method  
152 depends on several factors, including input composition, desired biogas quality, local  
153 market conditions, volume of biogas to be treated, and cost of the upgrading process.  
154 Water scrubbing (see **Figure 3a**) is the most commonly used technology in this  
155 respect,<sup>[23]</sup> involving around 41% of biogas upgrading plants worldwide.<sup>[22]</sup> The process  
156 involves directing the biogas through a column filled with a water-based scrubbing  
157 solution that selectively absorbs impurities. The impure water, containing traces of CH<sub>4</sub>,  
158 exits the column at the lower end and enters a flash tank whose pressure is lower than  
159 the feed pressure, resulting in the release of absorbed impurities. In this tank, the small  
160 amount of CH<sub>4</sub> is extracted and reintroduced into the scrubbing column for further  
161 purification. The aqueous solution is then directed to a desorption column for  
162 regeneration, with continuous recirculation through the column. It is worth noting that  
163 water scrubbing requires a large volume of water, a resource that can be scarce in some  
164 regions. In addition, the process can produce wastewater, which must be treated before  
165 proper disposal.

166 An alternative to water scrubbing is chemical absorption (see **Figure 3b**). Instead of  
167 water, a chemical solution such as an amine, is used. The amine solution removes  
168 impurities from the biogas, and it becomes saturated at the bottom of the column. After  
169 the heat exchanger, the solution passes into the desorption/stripping column, where the  
170 temperature is raised to between 100 and 180 °C for regeneration. The solvent saturated  
171 with contaminants is then treated to release the absorbed impurities. Besides amines,  
172 other alkaline salts such as sodium, potassium and calcium hydroxides can also be used.  
173 <sup>[23]</sup> The disadvantages of this method are that, firstly, the solvents used can be toxic to  
174 humans and the environment and, secondly, a significant amount of energy is required



175 to regenerate the chemical solutions, which can result in an energy expenditure of over  
176 20% of a power plant's total energy production.<sup>[24]</sup>

177 Cryogenic separation (see **Figure 3c**) is another technique that involves cooling  
178 biogas to very low temperatures to liquefy impurities, enabling their separation from the  
179 biogas stream according to their boiling point.<sup>[25]</sup> The use of cryogenic separation for  
180 biogas upgrading faces several challenges, including high initial investment and  
181 operating costs,<sup>[23]</sup> which limit the widespread adoption of this technique in industry.

182 Membrane separation (see **Figure 3d**) is another common method that involves  
183 using a semi-permeable membrane, allowing CH<sub>4</sub> to pass through while retaining  
184 impurities such as CO<sub>2</sub> and water vapor.<sup>[26]</sup> However, this technology has major  
185 disadvantages, including the high cost of membranes and their fragility.<sup>[23]</sup> Additionally,  
186 the economic viability of membrane separation processes has proved difficult for small-  
187 scale plants (< 100 Nm<sup>3</sup> h<sup>-1</sup> biogas flowrate).<sup>[22]</sup>

188 The last method is pressure swing adsorption (PSA) (see **Figure 3e**), which uses  
189 adsorbent materials to separate CO<sub>2</sub> and other impurities from the biogas stream. The  
190 adsorbent material is regenerated by reducing the pressure, releasing the impurities and  
191 leaving a concentrated CH<sub>4</sub> stream.<sup>[6]</sup> The popularity of PSA technology in biogas  
192 upgrading is growing due to its energy efficiency, low operating and installation costs,  
193 compact equipment design and user-friendly operation.<sup>[2]</sup>

194 **[Figure 3 here]**

### 195 ***2.3 Use of Sorbents in Biogas Upgrading***

196 Nanoporous materials are frequently considered the most suitable for biogas  
197 upgrading involving adsorption processes. Research on the removal of H<sub>2</sub>S from biogas  
198 has primarily concentrated on ACs<sup>[27-29]</sup> and zeolites.<sup>[30-32]</sup> In addition, other adsorbents,

199 including alumina, silica gel, along with ACs<sup>[33–35]</sup> and zeolites once more, have been  
200 used to eliminate siloxanes. CO<sub>2</sub>, the most common contaminant in biogas streams, has  
201 been mainly studied with ACs, CMSs, MOFs and zeolites (see **Tables S1** and **S2** in the  
202 Supplementary Information). **Table 2** gives an overview of some of the characteristics  
203 of these materials.

- 204 • ACs are a subject of extensive research due to their remarkable characteristics,  
205 including a large surface area, high micropore volume and appropriate pore size  
206 distribution (PSD).<sup>[36]</sup> ACs exhibit a relatively low heat of adsorption, translating  
207 to low energy requirements for regeneration. Additionally, ACs are generally  
208 cost-effective.<sup>[37]</sup>
- 209 • CMSs, as implied by their name, consist primarily of carbon, and they have  
210 demonstrated effectiveness in separating CO<sub>2</sub> from CH<sub>4</sub> due to their small pore  
211 size, enabling kinetically preferential adsorption for CO<sub>2</sub>. However, their  
212 production is expensive, and their performance may be restricted by a low  
213 adsorption capacity<sup>[38]</sup> (see **Table S2** of the Supplementary Information).
- 214 • MOFs have recently emerged as a promising class of materials, due to their high  
215 surface area and pore volume, which allow efficient gas adsorption and  
216 separation. MOFs can be tailored with specific pore sizes and shapes, enabling  
217 selective adsorption of CO<sub>2</sub> over CH<sub>4</sub>. However, a drawback of MOFs is their  
218 relatively low stability under certain conditions, such as high temperatures or  
219 humid environments.
- 220 • Zeolites, as porous crystalline aluminosilicates, exhibit a high selectivity for CO<sub>2</sub>  
221 and possess high CO<sub>2</sub> adsorption capacities (see again **Table S2** of the  
222 Supplementary Information). This can be attributed to their PSD and surface  
223 chemistry. Additionally, zeolites also have good thermal and chemical stability,

224 making them durable and suitable for prolonged usage. However, they also have  
225 some disadvantages with regard to the substantial adsorption heat of CO<sub>2</sub>, leading  
226 to challenges in adsorbent regeneration.<sup>[38]</sup>

227 **[Table 2 here]**

228 In the literature, the evaluation of adsorbents typically involves assessing their  
229 adsorption equilibrium with pure gases (e.g. CH<sub>4</sub> and CO<sub>2</sub>) or conducting breakthrough  
230 curve experiments using a synthetic gas mixture that mimics biogas composition (e.g.  
231 CH<sub>4</sub> = 65 vol. %, CO<sub>2</sub> = 35% vol. %). When considering the separation of CO<sub>2</sub> and CH<sub>4</sub>  
232 using a PSA process, it is important to consider not only the properties of the adsorbent  
233 but also the operational parameters of the PSA unit. Indeed, the adsorption capacity of  
234 the adsorbent and the efficiency of the separation process can be influenced by various  
235 factors such as feed gas flow rate, pressure, temperature, cycle time, as well as the type  
236 and amount of adsorbent used. A recommended approach for selecting an optimal  
237 adsorbent/PSA system configuration is to select adsorbents based on equilibrium  
238 isotherms and dynamic measurements to identify the most promising candidates.  
239 Subsequently, the chosen adsorbent undergoes evaluation in a PSA system to establish a  
240 set of baseline performance data. Finally, a reliable numerical model of the PSA process  
241 can be validated using experimental PSA data, enabling exploration of additional cycles  
242 and operating windows.<sup>[39]</sup>

### 243 **3. CO<sub>2</sub>/CH<sub>4</sub> Separation by Adsorption Processes**

#### 244 ***3.1 Adsorbents for CO<sub>2</sub>/CH<sub>4</sub> Separation***

245 The preferential selectivity of the components of a gas mixture for a given adsorbent  
246 is the fundamental principle behind adsorption/separation processes. Ideally, a high  
247 selectivity is needed, but a large working capacity ratio in the adsorption column is also

248 desirable as it determines the size and cost of the bed separation system.<sup>[40]</sup> In addition  
249 to the aforementioned selection criteria concerning adsorption and separation  
250 performance, various other factors associated with an adsorbent are of significant  
251 importance.<sup>[41]</sup> These include aspects such as ease of synthesis, density, scalability,  
252 sustainability, availability, physicochemical stability, cost, hydrophobicity, and  
253 toxicity.<sup>[24]</sup> The strength of the interaction between adsorbent and adsorbate is  
254 determined by the adsorption enthalpy. The adsorption enthalpy of CO<sub>2</sub> lies between -  
255 25 and -50 kJ mol<sup>-1</sup> for physisorption and is below -60 kJ mol<sup>-1</sup> for chemisorption. A  
256 higher enthalpy in absolute value requires more energy for CO<sub>2</sub> desorption, which  
257 increases regeneration costs. However, too low an enthalpy in absolute value results in  
258 low CO<sub>2</sub> adsorption capacity.<sup>[41]</sup>

259 The surface of an adsorbent material attracts gas molecules through a combination of  
260 Van der Waals interactions and electrostatic forces from more or less polar or  
261 quadrupolar species. CO<sub>2</sub> is a molecule with a quadrupole moment of  $13.4 \times 10^{-40} \text{ cm}^2$ ,  
262 whereas CH<sub>4</sub> has no polarity. Due to this significant difference in polarity, the presence  
263 of polar functional groups on the adsorbent surface proves highly beneficial in  
264 enhancing the selectivity for CO<sub>2</sub>.<sup>[42]</sup> These interactions vary in strength, enabling  
265 different substances to be adsorbed to varying extents. Separation of CO<sub>2</sub> based on this  
266 kind of electrostatic interactions with the adsorbent is called equilibrium separation.<sup>[41]</sup>  
267 When selectivity results from significant variations in the diffusivity of the different  
268 molecules in the micropores, the separation is called kinetic separation.

269 To identify the optimum adsorbent for selectively capturing CO<sub>2</sub> from biogas  
270 streams, various parameters can be considered, including BET area, micropore volume,  
271 adsorbent capacity at different CO<sub>2</sub> partial pressures for biogas upgrading, and CO<sub>2</sub>/CH<sub>4</sub>  
272 selectivity (see again **Table S1** and **Table S2** in the S.I). Porous materials used in

273 CO<sub>2</sub>/CH<sub>4</sub> separation by PSA units can be classified into carbonaceous materials such as  
274 ACs and CMSs, or other inorganic or hybrid materials such as zeolites or MOFs,  
275 respectively, see **Table 3**.

276 **[Table 3 here]**

### 277 *3.1.1 Carbon Adsorbents for CO<sub>2</sub>/CH<sub>4</sub> Separation*

278 ACs can be synthesized from a variety of precursors, including coal, char, peat,  
279 petroleum coke, lignite, wood and other biomass materials.<sup>[43]</sup> Additionally, industrial  
280 waste can serve as a viable source, provided it contains a high carbon content and  
281 minimal levels of inorganic compounds, commonly referred to as ashes.<sup>[44]</sup> The  
282 preparation of ACs involves enriching the raw material with carbon through heat  
283 treatment and developing and opening porosity, which corresponds to the activation  
284 process itself. There are two primary activation processes: physical activation, which  
285 involves carbon dioxide<sup>[36, 37, 44–46]</sup> and/or water vapor<sup>[36]</sup> as gasifying agents, and  
286 chemical activation, which involves the use of substances such as phosphoric acid  
287 (H<sub>3</sub>PO<sub>4</sub>),<sup>[47–49]</sup> potassium hydroxide (KOH),<sup>[3, 47, 50–53]</sup> or potassium carbonate  
288 (K<sub>2</sub>CO<sub>3</sub>),<sup>[49, 54]</sup> amongst others.

289 Physical activation enhances the textural characteristics of the resulting carbon by  
290 creating micropores, thereby increasing its adsorption capacity. Furthermore, physical  
291 activation can enlarge existing porosity by making micropores wider and introducing  
292 some mesoporosity into the carbon structure, which facilitate molecules diffusion within  
293 carbon.<sup>[55]</sup> Finally, it also facilitates the emergence of oxygenated functional groups,  
294 including phenolic, ketonic, and carboxylic groups,<sup>[43]</sup> which may enhance carbon  
295 surface interaction with molecules. Physical activation processes involve progressive  
296 carbon gasification, limiting control over micropore size distribution. In contrast,

297 chemical activation methods offer a good alternative, as they enable porosity  
298 development to be precisely controlled and modified. Through well-controlled  
299 activation conditions, the porosity characteristics of the carbon material can be  
300 significantly altered, leading to tailored and optimized PSDs.<sup>[55]</sup> Nevertheless, chemical  
301 activation is often considered detrimental to the environment, given the use of water to  
302 dissolve reagents, extract and wash products, separate mixtures, clean reaction  
303 apparatus, and disperse products for practical applications.<sup>[44]</sup> It is important to  
304 recognize, however, that the surface area of chemically and physically activated carbons  
305 can be influenced by a variety of factors, including the precursor material and other  
306 activation conditions.

307 The incorporation of heteroatoms such as nitrogen, phosphorus, and sulfur has been  
308 investigated to further enhance the properties of activated carbons.<sup>[53]</sup> Nitrogen-  
309 functionalized ACs, in particular, have shown improved CO<sub>2</sub> adsorption capacity and  
310 selectivity through mechanisms such as acid-base interactions and hydrogen bonding.<sup>[24]</sup>  
311 Incorporating heteroatoms, such as nitrogen, into the carbon framework can  
312 significantly enhance adsorption efficiency by improving interactions between gas  
313 molecules and carbon. Reported nitrogen-doped activated carbons with very high  
314 surface areas, exceeding 1400 m<sup>2</sup>·g<sup>-1</sup>, have confirmed the improvement achieved by this  
315 approach.<sup>[24, 56]</sup>

316 It is feasible to create carbon adsorbents with tightly controlled PSDs in their porous  
317 structures. These materials, known as CMSs, possess narrow, uniformly sized  
318 micropores that are able to sieve molecules based on their differences in diffusion rate,  
319 size and shape.<sup>[57]</sup> The CMS production process can be similar to the preparation of  
320 ACs, but with an additional step involving pore shrinkage. This is achieved by  
321 controlled deposition of carbon obtained by high-temperature cracking of molecules

322 such as benzene or acetylene.<sup>[40]</sup> CMSs can also be produced by controlled pyrolysis of  
323 synthetic polymers such as polyvinylidene chloride, polyimide and phenol-  
324 formaldehyde resin.<sup>[58]</sup> By carefully adjusting the preparation conditions, a highly  
325 homogeneous PSD can be obtained.<sup>[40]</sup>

326 CMSs exhibit uniform, slit-shaped pore openings, similar in size to those of small  
327 molecules (N<sub>2</sub>, O<sub>2</sub>, CO<sub>2</sub> or CH<sub>4</sub>). It is essential for a CMS to possess pore sizes between  
328 3.2 and 3.7 Å to ensure the sieving effect,<sup>[6]</sup> which implies that small gas molecules pass  
329 through the narrow channels and pores more easily than larger molecules. For instance,  
330 since the CH<sub>4</sub> molecule (3.8 Å) is larger than that of CO<sub>2</sub> (3.3 Å), the latter is more  
331 adsorbable. The main difference between ACs and CMSs lies in their PSD. ACs exhibit  
332 a disordered and widely distributed range of pore sizes, from 0.4 to 4 nm and often  
333 extending far beyond this range. This characteristic renders them unsuitable for the  
334 kinetic separation of gas mixtures, as their broad PSD hampers their kinetically-based  
335 selectivity.<sup>[6]</sup> CMSs have the potential to facilitate highly effective kinetic separation,  
336 relying on differences in sorption rates rather than sorption equilibrium. Nonetheless,  
337 CMS synthesis requires the modification of the pores of the carbon precursor, involving  
338 energy-intensive and complex techniques such as chemical vapor deposition (CVD).  
339 Consequently, conventional CMSs may not be suitable for household biogas upgrading  
340 systems due to their cost-effectiveness limitations.<sup>[14]</sup>

341 If ACs exhibit stronger surface interactions with CO<sub>2</sub>, allowing them to adsorb larger  
342 quantities of this gas compared to CH<sub>4</sub>, CMSs are kinetic-based adsorbents. CMSs  
343 control the diffusion rate thanks to their narrow micropore size, resulting in greater CO<sub>2</sub>  
344 retention per unit time.<sup>[59]</sup> Due to these kinetics restrictions, CMSs use only a fraction of  
345 their total adsorption capacity.

### 346 3.1.2 Other Adsorbents for CO<sub>2</sub>/CH<sub>4</sub> Separation

347 MOFs are produced by the self-assembly of organic ligands consisting of  
348 carboxylate, phosphonate, pyridyl and imidazolate or other azolate functional groups  
349 and metal oxide clusters (e.g. Cu<sup>2+</sup>, Mg<sup>2+</sup>, Al<sup>3+</sup>, Cr<sup>3+</sup> or Zn<sup>2+</sup>),<sup>[60]</sup> resulting in the  
350 formation of crystalline structures with exceptionally high surface areas and pore  
351 volumes. MOFs have a very regular porous structure with adjustable pore sizes and  
352 chemical functionalities that can be customized by modifying the metal groups or  
353 organic ligands.<sup>[61]</sup>

354 MOFs typically exhibit surface areas exceeding 4000 m<sup>2</sup>·g<sup>-1</sup>,<sup>[62]</sup> surpassing those  
355 observed in conventional porous materials. Within MOFs, CO<sub>2</sub> adsorption is enhanced  
356 by the metal sites, capable of inducing local electric field effects, thereby increasing the  
357 affinity for CO<sub>2</sub> in comparison to CH<sub>4</sub>.<sup>[63]</sup> Furthermore, strategic functionalization, such  
358 as incorporating polyamines to introduce CO<sub>2</sub>-binding sites through physical means, or  
359 integrating carbon nanotubes and chemically decorating them with amine groups have  
360 allowed to further increase CO<sub>2</sub> adsorption selectivity over CH<sub>4</sub>.<sup>[63]</sup> Thus, CO<sub>2</sub>-MOF  
361 interactions can be adjusted through the use of functionalized ligands. Among the  
362 functional groups most commonly incorporated into MOF ligands are thiols, carbonyls,  
363 carboxyls, cyano groups and amines.<sup>[60]</sup>

364 One of the primary drawbacks of MOFs is their limited stability to water at moderate  
365 to high temperature,<sup>[64]</sup> which can, however, be improved by both post-synthetic  
366 modifications and material compounding.<sup>[63]</sup> While MOFs have proven effective, their  
367 complex preparation methods often make the process uneconomical. It is therefore  
368 necessary to develop new, economically viable compounds that can be synthesized by  
369 solvent-free reactions or by simple precipitation reactions under ambient conditions.<sup>[60]</sup>



370 Among all the MOFs, the most remarkable and cutting-edge one for CO<sub>2</sub> adsorption  
371 is a zinc-based one developed at the University of Calgary, known as CALF-20. This  
372 MOF exhibits a high capacity for adsorbing CO<sub>2</sub> while also showcasing selectivity over  
373 water. CALF-20 demonstrates competitive separations by favoring CO<sub>2</sub> physisorption at  
374 relative humidity levels below 40%. Computational modeling supports this observation.  
375 CALF-20 imposes a low enthalpic regeneration penalty and demonstrates robustness  
376 against steam (> 450,000 cycles) and wet acid gases. Notably, its preparation involves a  
377 single-step process, enabling formation of composite materials, and its synthesis can be  
378 scaled up to produce multikilogram batches.<sup>[65]</sup>

379 MOFs have attracted attention for their remarkable CO<sub>2</sub> adsorption capacities,  
380 reaching values as high as 33.5 mol kg<sup>-1</sup> at 35 bar. However, for applications such as  
381 biogas upgrading, good adsorption capacity is best achieved at lower pressures (< 10  
382 bar). Indeed, compression up to 35 bar requires more expensive equipment and  
383 increases energy costs. MOFs with high adsorption capacity at high pressures are less  
384 suited to the lower pressure ranges (< 5 bar), where zeolites generally have higher  
385 adsorption capacities.<sup>[41]</sup> One area of ongoing research in MOFs is CO<sub>2</sub> diffusion, which  
386 has been reported to be poor,<sup>[66]</sup> for instance with MIL-53,<sup>[67]</sup> where reduced diffusion  
387 has been attributed to the presence of hydroxy groups within its structure. On the other  
388 hand, in another study, it was reported that in the case of MIL-53 there were no  
389 significant mass transfer limitations.<sup>[68]</sup>

390 Zeolites are crystalline, microporous materials composed of hydrated  
391 aluminosilicates with a three-dimensional framework structure. They consist of a  
392 network of tetrahedra (aluminum, silicon, and oxygen) that create cavities and channels  
393 of a uniform size and shape. These materials possess a high surface area and regularly  
394 spaced pores, allowing them to selectively adsorb and desorb molecules based on size

395 and polarity.<sup>[64]</sup> Renowned for their molecular sieving capabilities, zeolites possess  
396 highly selective properties, effectively excluding molecules beyond a critical size and  
397 restraining the diffusion of molecules nearing this threshold. This separation  
398 mechanism, commonly referred to as steric separation, along with the effects of kinetic  
399 separation, offers reliable and predictable gas separation.<sup>[40]</sup> Medium- and large-pore  
400 zeolites achieve equilibrium separation. On the other hand, the selectivity of the  
401 separation process in small-pore zeolites is generally affected by the diffusion rate of  
402 adsorbates in the pores. Due to its smaller kinetic diameter than CH<sub>4</sub>, CO<sub>2</sub> exhibit  
403 higher diffusion rates than CH<sub>4</sub> through several small-pore zeolites. This difference may  
404 have an impact diffusion through narrow pores more than on the interaction of the  
405 molecules with the zeolite surface, particularly in low-Al zeolites.<sup>[41]</sup>

406 The efficiency of zeolites for CO<sub>2</sub> capture also depends on their chemical  
407 composition and charge density.<sup>[64]</sup> In general, the separation capability improves as the  
408 electrostatic field in the zeolite cavities intensifies, which is mainly influenced by the  
409 charge of the framework and can be altered by the type of charge-compensating cations  
410 or the Al content in the zeolite framework.<sup>[69]</sup> Zeolite performance is also adversely  
411 affected by the presence of moisture, which can significantly decrease the amount of  
412 CO<sub>2</sub> adsorbed on the zeolite surface. Indeed, moisture can react with adsorbed CO<sub>2</sub>  
413 molecules to form an adsorbed layer that prevents access to other CO<sub>2</sub> molecules.<sup>[4]</sup>

414 SAPO-56 (Silicoaluminophosphate-56), ZSM-5 (Zeolite Socony Mobil-5) and  
415 Sodalite-based Zeolites, like Na-X and Na-A, among others, have been studied for their  
416 potential in CO<sub>2</sub> separation processes due to their versatile pore structures and  
417 adsorption properties. The adsorption capacity of zeolite NaX, also called zeolite X,  
418 NaX, Linde X and molecular sieve 13X, is among the highest for zeolites (6.3 mmol·g<sup>-</sup>  
419 <sup>1</sup>), and this can be further improved by ion exchange.<sup>[41]</sup> However, zeolite NaX strongly

420 interacts with water molecules, to the extent that it is marketed as a desiccant.<sup>[70]</sup> When  
421 water is adsorbed close to its saturation point, its CO<sub>2</sub> capacity decreases significantly,  
422 being an order of magnitude lower compared to dry material.<sup>[71]</sup> The working capacities  
423 and CO<sub>2</sub>/CH<sub>4</sub> selectivities of some of these zeolites, when used in PSA systems, will be  
424 examined in the next section.

### 425 **3.2 CO<sub>2</sub>/CH<sub>4</sub> Separation by Pressure Swing Adsorption**

426 Several types of PSA cycles with distinct advantages and limitations exist, depending  
427 on the specific application and gas separation requirements. Given the potential  
428 confusion in the nomenclature of different cycles, such as the Vacuum Swing  
429 Adsorption process, commonly referred to as VSA or VPSA, we have used the  
430 following nomenclature for PSA cycles in the remainder of this article:

- 431 • *PSA*: pressure swing adsorption (Skarstrom cycle)
- 432 • *VSA*: vacuum swing adsorption (cycle with sub-atmospheric depressurization  
433 without pressure equalization)
- 434 • *EPSA*: equalization pressure swing adsorption (cycle with pressure equalization,  
435 without sub-atmospheric depressurization)
- 436 • *EVSA*: equalization vacuum swing adsorption (cycle with pressure equalization  
437 and sub-atmospheric depressurization)

438 **Figure 4** illustrates the conventional cycles involved in PSA and the corresponding  
439 pressure variations. Specifically, **Figure 4a** shows the Skarstrom PSA cycle. In the  
440 initial phase, bed 2 is pressurized to the adsorption pressure ( $P_a$ ) with gas feed  
441 (CO<sub>2</sub>+CH<sub>4</sub>), while bed 1 is blowdown to atmospheric pressure. Subsequently, the high-  
442 pressure feed then flows through bed 2, where the most strongly adsorbed component is  
443 retained in the bed. A gas stream enriched with the least strongly adsorbed component  
444 exits as effluent at a pressure slightly below that of the feed. Most of the effluent stream

445 is withdrawn as the product, and a fraction is used to purge bed 1 at low operating  
446 pressure. The subsequent two steps follow an identical sequence, but with the  
447 interchange of beds. **Figure 4b** also presents the pressure equalization cycle, wherein  
448 bed 2 is initially pressurized with gas sourced from the outlet region of bed 1. Following  
449 pressure equalization, the two beds are disconnected, and bed 2 undergoes  
450 pressurization with feed gas, while bed 1 is vented to complete blowdown. The  
451 subsequent phases of the Skarstrom cycle proceed normally, with the exception that  
452 during the regeneration phase, bed 2 undergoes partial depressurization by connecting  
453 to the previously depressurized bed 1. It should be noted that the pressure equalization  
454 step interrupts the feed, and if a continuous feed is required, two additional beds are  
455 needed.

456 **[Figure 4 here]**

457 In order to select the most suitable adsorbent for PSA operation, several factors are  
458 considered, including its gas separation properties under both equilibrium and dynamic  
459 conditions, ease of regenerability and operating costs. Two key properties, namely  
460 adsorbent selectivity and PSA working capacity ratio, are analyzed in detail as they  
461 significantly influence adsorbent efficiency in the PSA process.

### 462 3.2.1 Adsorption Selectivity (*dimensionless*)

463 The adsorption selectivity ( $S$ ) is defined as follows:

$$S = \frac{X_{CO_2} \cdot Y_{CH_4}}{X_{CH_4} \cdot Y_{CO_2}} \quad (1)$$

464 where  $X$  refers to the molar fraction of a given compound in the adsorbed state, and  $Y$  is  
465 the molar fraction of this compound in the gas phase. The Ideal Adsorption Solution  
466 Theory (IAST), introduced by Myers and Prausnitz,<sup>[72]</sup> is a tool utilized to predict the

467 adsorption behavior of individual components in a gas mixture. IAST relies on three  
 468 fundamental assumptions that enable a simplified and accurate representation of  
 469 complex adsorption phenomena:<sup>[52]</sup> a) thermodynamic inertness of the adsorbent, (b)  
 470 adsorption of the mixture as an ideal solution under given temperature and pressure  
 471 conditions, and (c) the equivalence of chemical potential for the adsorbed and gas  
 472 phases.

473 For calculations with this model, the system of equations includes the relationships  
 474 linking the behavior of molecules in the gas state with their behavior when adsorbed.  
 475 The relationship between the pure component adsorption isotherms and of the so-called  
 476 reduced spreading pressure is defined as:<sup>[73]</sup>

$$\frac{\pi A}{RT} = \int_0^{p_i^0} \frac{n_i^0}{p} dp \quad (2)$$

477 where  $\pi$  is the spreading pressure,  $A$  is the surface area,  $i$  represents the molecule under  
 478 consideration and  $p_i^0$  is the is the saturated vapour pressure exerted by component  $i$  in  
 479 its pure state at the same temperature and spreading pressure of the adsorbed state.<sup>[74]</sup>  
 480 The term  $n_i^0$  can be calculated by the appropriate pure component isotherm, in this case  
 481 the Toth isotherm equation:<sup>[72]</sup>

$$n_i^0 = n_{i,max} \cdot \frac{f_i \cdot p_i}{[1 + (f_i \cdot p)^t]^{\frac{1}{t}}} \quad (3)$$

482  $n_i^0$  (mol kg<sup>-1</sup>) and  $n_{i,max}$  (mol kg<sup>-1</sup>) represent the adsorption capacity of the adsorbent at  
 483 equilibrium pressure and the maximum adsorption capacity when the adsorbent is fully  
 484 saturated, respectively, and  $p$  (Pa) is the equilibrium pressure. The parameters  $f$  and  $t$  are  
 485 specific to adsorbate-adsorbent pairs. The Toth model proved its effectiveness in fitting  
 486 the experimental data within the specified operating range for most of adsorbents. In  
 487 some cases, the dual-site Langmuir adsorption model was applied for a better fit.

488 Nevertheless, it has been concluded that the IAST predictions are unaffected by the  
489 specific equation chosen for fitting the pure gas isotherms. The crucial criterion is a  
490 high-quality alignment between the experimental data of single gas and those calculated  
491 using the selected model.<sup>[36]</sup>

492 The relationship between the mole fractions in the gas phase and in the adsorbed  
493 phase is:

$$Y_i \cdot p = X_i \cdot p_i^o \quad (4)$$

494 where  $Y_i$  is the mole fraction of component  $i$  in the gas phase and  $X_i$  is the mole fraction  
495 of component  $i$  in the adsorbed phase. After solving this system of equations, all the  
496 molar fractions within the adsorbed phase are calculated. Using the parameters  $n_i^0$ ,  
497 which are the adsorbed amounts for the pure components for the same pressure range as  
498 in the mixture, the total amount adsorbed is determined by:

$$\sum_{i=1}^k \frac{X_i}{n_i^0} = \frac{1}{\sum_{i=1}^k n_i} \quad (5)$$

499 The system of equations is then solved by Newton's method using 3P Sim software.  
500 The IAST multicomponent adsorption approach was applied to analyze experimental  
501 data from a range of adsorbents documented in the literature (see **Tables S1** and **S2** in  
502 the Supporting Information).

### 503 3.2.2 PSA Working capacity ratio (dimensionless)

504 The PSA working capacity ratio,<sup>[75, 76]</sup> represents the ratio of the amount of gas that  
505 can be adsorbed and desorbed during a single adsorption-desorption cycle under  
506 specific adsorption and desorption operating pressures at a given temperature. For the  
507 gas analyzed, comprising CO<sub>2</sub> and CH<sub>4</sub> at given contents (e.g., 35% CO<sub>2</sub> and 65 %  
508 CH<sub>4</sub>), the mixture adsorption isotherms must be known to determine the amounts  
509 adsorbed at each operating pressure, as expressed by the following equation:

$$PSA \text{ working capacity ratio} = \frac{CO_2 \text{ adsorbed @ } P_a - CO_2 \text{ adsorbed @ } P_d}{CH_4 \text{ adsorbed @ } P_a - CH_4 \text{ adsorbed @ } P_d} \quad (6)$$

510 where  $P_a$  is the adsorption pressure and  $P_d$  the desorption pressure of the PSA cycle.  
511 The working capacity ratio and selectivity of adsorbents are common criteria that  
512 determine the capital and operating costs of the biogas upgrading process. For instance,  
513 a high adsorption working capacity ratio can reduce the amount of adsorbent required  
514 by the PSA system.<sup>[39]</sup>

515 Adsorption pressure depends on the cycle applied during the process. VSA cycles  
516 generally operate at  $P_a$  between 1 and 2 bar, with regeneration taking place under  
517 vacuum. On the other hand, for PSA cycle or any other cycle with regeneration at  
518 atmospheric pressure,  $P_a$  is generally between 3 and 7 bar. In order to evaluate the cases  
519 for regeneration at atmospheric and sub-atmospheric pressure, two hypothetical  
520 scenarios were examined: (1) a PSA cycle with  $P_a = 5$  bar and  $P_d = 1$  bar, and (2) a  
521 VSA cycle with  $P_a = 1$  bar and  $P_d = 0.2$  bar. For the VSA cycle, pure component  
522 isotherms from the literature reporting pressures up to 1 bar were analyzed, while  
523 experimental isotherms at higher pressures were studied for both VSA and PSA cycles.  
524 Both scenarios were run at an operating temperature of approximately 25 °C. The  
525 results are presented in **Figure 5**.

526 The adsorption isotherms for the binary gas mixture (e.g. 35% CO<sub>2</sub> and 65 % CH<sub>4</sub>)  
527 are lower than those for the pure components, indicating a significant impact of the gas  
528 mixture on adsorption performance. This is primarily due to the reduction in partial  
529 pressures of the individual components upon mixing. The presence of CO<sub>2</sub>, which has a  
530 high adsorption propensity, leads to a significant decrease in the adsorption of CH<sub>4</sub>,  
531 which is relatively poorly adsorbed.<sup>[36]</sup>

532 **[Figure 5 here]**

533 Clearly, zeolites perform the best under both atmospheric and sub-atmospheric  
534 depressurization conditions. Zeolites with precisely determined micropores<sup>[40]</sup> are much  
535 more selective than carbonaceous adsorbents. Moreover, zeolites generate an  
536 electrostatic force that enhances CO<sub>2</sub> capture.<sup>[77]</sup> Although N-doped ACs provide a  
537 considerable improvement over other ACs, such as N-WAPC,<sup>[53]</sup> which is the second  
538 best-performing AC, they are still far from competitive with zeolites. P-AC<sup>[47]</sup> is the AC  
539 that appears to be highly effective and relatively competitive with zeolites. This AC was  
540 derived from coconut shells and subjected to chemical activation by impregnation with  
541 a phosphoric acid solution. It was then carbonized at a temperature of 600 °C, resulting  
542 in a BET area of 1922 m<sup>2</sup>·g<sup>-1</sup> and a micropore volume of 0.68 cm<sup>3</sup>·g<sup>-1</sup>, which are  
543 exceptional characteristics that make it a promising candidate. Surprisingly, despite its  
544 impressive performance, to the best of our knowledge, there are no studies exploring its  
545 potential as an innovative adsorbent for CO<sub>2</sub>/CH<sub>4</sub> separation.

546 Zeolites exhibit the highest performance among materials; however, their high heat  
547 of adsorption poses a challenge for regeneration, requiring very low sub-atmospheric  
548 pressure and increased energy consumption. This drawback of zeolites may create an  
549 opportunity for MOFs, which exhibit superior performance compared with ACs and  
550 CMSs. The heat of adsorption for CO<sub>2</sub> in MOFs has been reported at -30 kJ·mol<sup>-1</sup>,<sup>[61]</sup> a  
551 value similar to that observed for ACs, of around -28 kJ·mol<sup>-1</sup>,<sup>[45]</sup> and is significantly  
552 lower in absolute values than that observed in zeolites, which can vary between -42 and  
553 -63 kJ·mol<sup>-1</sup>.<sup>[78]</sup> Although CMSs have low selectivity, comparable to that of ACs, their  
554 driving force for CO<sub>2</sub>/CH<sub>4</sub> separation arises not only from adsorption equilibrium but  
555 also from adsorption kinetics. Therefore, their performance in adsorption columns is  
556 enhanced and competitive, as will be demonstrated in the next section. The data also  
557 indicate that lower working pressures result in much higher selectivity and working



558 capacity. This is because, at low pressures, the adsorbent material generally has a large  
 559 number of unoccupied adsorption sites. As the pressure increases, more and more sites  
 560 become occupied, and the availability of unoccupied sites decreases. This leads to a  
 561 lower adsorption rate as pressure increases. Consequently, the PSA process would work  
 562 best at a  $P_a$  of around 1 to 2 bar and, due to regeneration requirements, and optimum  
 563 desorption conditions for this process would require sub-atmospheric pressure.

#### 564 **4. PSA Units for CO<sub>2</sub>/CH<sub>4</sub> Separation**

##### 565 **4.1 Parameters for PSA Performance Evaluation**

566 Most studies on PSA units primarily focus on final purity and recovery, while little  
 567 attention is paid to productivity and energy consumption. While ensuring that the  
 568 separated gas meets the required purity specifications is essential, it is equally important  
 569 to consider the overall efficiency of the process. The productivity and energy  
 570 consumption of a PSA unit can significantly impact its economic feasibility and  
 571 sustainability. Therefore, to ensure that PSA units are both cost-effective and  
 572 environmentally friendly, it is crucial to optimize parameters such as productivity and  
 573 energy consumption, in addition to purity and recovery. To this end, it is useful to  
 574 examine the purity-recovery-productivity and purity-recovery-energy consumption  
 575 curves when comparing different process cycles and adsorbents. These parameters can  
 576 be obtained or calculated using the information provided in each paper from the  
 577 literature, using the following equations:

$$578 \quad \textbf{Purity:} \quad CH_4 \text{ Purity (\%)} = \frac{CH_4 \text{ recovered in the raffinate}}{\text{Total amount of the produced raffinate}} \times 100 \quad (7)$$

$$579 \quad \textbf{Recovery:} \quad CH_4 \text{ Recovery (\%)} = \frac{CH_4 \text{ recovered in the raffinate}}{\text{Total amount of gas feeding the system}} \times 100 \quad (8)$$

$$580 \quad \textbf{Productivity:} \quad \text{Productivity} = \frac{CH_4 \text{ recovered in the raffinate}}{\text{Amount of adsorbent} * \text{Cycle time}} \quad (9)$$

581 **Energy consumption:** Most energy consumption in PSA separation processes takes  
582 place during the compression stage and blowdown, particularly in the blower  
583 (compressor) and vacuum pump. The work needed for adiabatic gas compression from  
584 suction pressure,  $P_1$ , to discharge pressure,  $P_2$ , can be calculated using the following  
585 equation: [59, 79, 80]

$$W_s = \dot{n} \cdot R \cdot T \cdot \left( \frac{k}{k-1} \right) \cdot \left( \left( \frac{P_2}{P_1} \right)^{\frac{k-1}{k}} - 1 \right) \cdot \left( \frac{1}{\eta} \right) \quad (1)$$

586 where  $\dot{n}$  is the molar flow rate ( $\text{mol} \cdot \text{s}^{-1}$ ),  $R$  is the universal gas constant ( $\text{J} \cdot \text{K}^{-1} \cdot \text{mol}^{-1}$ ),  $T$   
587 is the temperature of the gas (K),  $k$  is the heat capacity ratio ( $C_p/C_v \approx 1.3$ ) of the gas  
588 mix, and  $\eta$  represents the mechanical efficiency, which is assumed to be 0.8. [38, 59]

#### 589 **4.2 Simulation of PSA systems**

590 Effective modelling and simulation of PSA systems is important for optimizing  
591 performance and scaling up industrial applications. This involves a dynamic  
592 mathematical model that includes the interaction between fluid flow and mass transfer  
593 processes. The simulation repeatedly solves the governing equations using numerical  
594 integration to determine the time-dependent behaviour of the variables. The governing  
595 equations include: mass balance, energy balance and momentum balance equations,  
596 moreover the adsorption onto the adsorbent is described by the adsorption isotherms  
597 and kinetics. **Table 4** summarizes the mathematical models implemented for the  
598 simulation of PSA units for  $\text{CO}_2/\text{CH}_4$  separation to produce high-purity methane.

599 **[Table 4 here]**

- 600 • Mass balance equation

601 All approaches apply the axially dispersed plug flow (ADPF) model to describe  
602 the fluid flow as presented in Eq. 11. [40]

$$-D_L \frac{\partial^2 c_i}{\partial Z^2} + \frac{\partial}{\partial Z}(v c_i) + \frac{\partial c_i}{\partial t} + \frac{1 - \varepsilon}{\varepsilon} \frac{\partial \bar{q}_i}{\partial t} = 0 \quad (11)$$

603 where  $D_L$  is the axial dispersion coefficient,  $c_i$  is the concentration of the component  $i$  in  
604 the gas phase,  $Z$  is the axial position along the column,  $v$  is the gas superficial velocity,  $t$   
605 is the time,  $\varepsilon$  is the bed porosity and  $\bar{q}_i$  is the average concentration of adsorbed  
606 component  $i$ . Fluid flow through a packed bed tends to cause axial mixing, which  
607 reduces separation efficiency, making its minimization a key design objective.<sup>[40]</sup> Two  
608 main mechanisms contribute to axial dispersion: molecular diffusion and turbulent  
609 mixing resulting from the splitting and recombination of flows around the adsorbent  
610 particles.<sup>[81]</sup> The ADPF model combines these mechanisms into a single effective axial  
611 dispersion coefficient ( $D_L$ ). More detailed models, including radial dispersion, are  
612 generally unnecessary and when mass transfer resistance is significantly greater than  
613 axial dispersion, it can be ignored, assuming ideal plug flow (IPF). This IPF assumption  
614 has been applied in some PSA separation processes, such as CH<sub>4</sub> enrichment in CH<sub>4</sub>/N<sub>2</sub>  
615 mixtures,<sup>[82]</sup> high-purity N<sub>2</sub> production from air,<sup>[83]</sup> and H<sub>2</sub> production by methane  
616 steam reforming.<sup>[84]</sup> Although in some small-scale lab systems, the axial dispersion of  
617 the flow can be neglected, when numerically solving the system of partial differential  
618 equations, it is easier to use the ADPF model as the inclusion of the axial dispersion  
619 term eliminates discontinuities in the slope of the concentration profile.<sup>[40]</sup>

620 The ADPF model is preferred to the ideal plug flow model for its realistic  
621 dispersion, its better prediction of the breakthrough curve, its consideration of non-ideal  
622 column packing, its accurate resistance to mass transfer, and its suitability to scale up  
623 from laboratory to industry. The ADPF model does not take radial variations into  
624 account, resulting in a 1-dimensional model, which also facilitates its numerical  
625 solution.<sup>[85]</sup> For these reasons, the ADPF model has consistently been used for CH<sub>4</sub>/CO<sub>2</sub>  
626 separation simulation.

627 • Equilibrium isotherm

628 In all simulation studies, the multisite Langmuir model (MLM), presented in Eq. 12,  
 629 which is the simplest model for describing multicomponent adsorption, <sup>[72]</sup> has been  
 630 used to predict the mixture isotherm. This model is preferred to the IAST equations as it  
 631 offers explicit expressions for the adsorbed phase concentrations, thus eliminating the  
 632 need for iteration during simulation. In contrast, the more accurate IAST equations are  
 633 implicit and require an iterative subroutine to determine the composition of the  
 634 adsorbed phase at equilibrium, which increases computation time.

$$\frac{q_i}{q_{si}} = \frac{1 + b_i P_i}{1 + b_i P_i + b_j P_j} \quad (12)$$

635 where  $q_i$  is the amount of component  $i$  adsorbed per unit mass of adsorbent,  $q_{si}$  is the  
 636 saturation capacity of the adsorbent for component  $i$ ,  $b_i$  is the Langmuir adsorption  
 637 equilibrium constant and  $P_i$  is the partial pressure of the component  $i$  in the gas phase.  
 638 Additionally, if the MLM does not fit well, as can occur at CO<sub>2</sub> concentrations above  
 639 39%, <sup>[86]</sup> the Extended Langmuir-Freundlich equation (see Eq. 13) <sup>[81]</sup> can be employed  
 640 as an alternative. This model introduces a power expression,  $m$ , making it effective for  
 641 correlating binary equilibrium data in simulation studies.

$$\frac{q_i}{q_{si}} = \frac{1 + b_i P_i^{m_i}}{1 + b_i P_i^{m_i} + b_j P_j^{m_j}} \quad (13)$$

642 • Rate of adsorption

643 Instantaneous equilibrium in an adsorption bed can only be assumed if all mass  
 644 transfer resistances are negligible. Since this is rarely the case, a specific rate expression  
 645 must be used to calculate the adsorbed amount ( $\bar{q}_i$ ). The resistances to adsorption are  
 646 interparticle transport (external to the particles), which occurs in series with intraparticle  
 647 transport (within the particles), <sup>[87]</sup> so the mass flow from fluid to solid is modelled  
 648 requiring a method to determine the mass transfer coefficient. Pore diffusion models

649 have been used to simulate PSA systems, <sup>[88]</sup> but the simpler and faster linear driving  
 650 force (LDF) model is more commonly applied, as seen in several cases in this work <sup>[68,</sup>  
 651 <sup>86, 89–93]</sup> and presented in Eq. 14:

$$\frac{\partial q_i}{\partial t} = k_i(q_i^* - q_i) \quad (14)$$

652 where  $k_i$  is the rate constant for adsorption of component  $i$ ,  $q_i^*$  is the amount adsorbed  
 653 at equilibrium under current conditions and  $q_i$  is the amount currently adsorbed.

654 A bi-LDF model <sup>[94]</sup> has also been proposed to approximate mass transfer  
 655 resistance in macropores and micropores using linear models. <sup>[59, 95–97]</sup> For macropores,  
 656 which involve both Knudsen and molecular diffusion, an effective LDF rate constant is  
 657 employed to combine transport through the external fluid film and within the  
 658 macropores, as presented in Eq. 15:

$$\varepsilon_p \frac{\partial c_i}{\partial t} + \rho_p \frac{\partial q_i}{\partial t} = \varepsilon_p \frac{15D_{pa,i}}{(R_p)^2} \times \frac{Bi_i}{Bi_i + 1} (C_i - c_i) \quad (15)$$

659 where  $\varepsilon_p$  is the particle porosity,  $\rho_p$  is the particle density,  $D_{pa,i}$  is the macropore  
 660 diffusivity of component  $i$ ,  $Bi_i$ , is the Biot number of the component  $i$ , which represents  
 661 the ratio of the internal resistance of the macropores to the resistance of the external  
 662 film,  $C_i$  is the gas concentration of component  $i$  and  $c_i$  is the average concentration in  
 663 the macropores for component  $i$ .

664 In the micropores, the Darken equation is used to account for the concentration  
 665 dependence of micropore diffusivity.

$$\frac{\partial q_i}{\partial t} = \frac{15D_{p,i}}{(R_c)^2} (q_i^* - q_i) \quad (16)$$

666 where  $D_{p,i}$  is the micropore diffusivity of component  $i$ , also called “crystal diffusivity”  
 667 in the case of zeolites. <sup>[94]</sup> When separation is governed by equilibrium rather than  
 668 kinetics, mass transfer resistance does not affect the process significantly and the spread  
 669 of the mass transfer zone along the adsorption column is mainly due to axial dispersion.

670           • Gas phase behaviour

671       The behaviour of bulk gas is modelled in most of cases using the ideal gas law,  
672 except in the work of De Witte et al. <sup>[92]</sup>, where the Peng-Robinson equation, was  
673 applied and in the study of Grande et al., where experiments at pressures as high as 80  
674 bar where conducted. <sup>[95]</sup> In this high-pressure case, the Benedict-Webb-Rubin (BWR)  
675 equation was employed to account for deviations from ideal gas behaviour. The  
676 assumption of the ideal gas law, where the compressibility factor ( $z$ ) is equal to 1, can  
677 lead to inaccuracies in modelling, particularly at high pressures and low temperatures.  
678 To illustrate the impact of operating conditions on CO<sub>2</sub>/CH<sub>4</sub> separation, **Figure 6** shows  
679 the variation in the compressibility factor ( $z$ ) from the ideal gas assumption. In Fig. 6, 1  
680 -  $z$ , is calculated using the NIST Reference Fluid Thermodynamic and Transport  
681 Properties Database (REFPROP-version 10.0). <sup>[98]</sup>

682       **[Figure 6 here]**

683       At a common operating pressure of 10 bar and a temperature of 25 °C, the  
684 compressibility factor for CO<sub>2</sub> is 0.95, resulting in a delta  $z$  of 0.05. For CH<sub>4</sub>,  $z = 0.98$ ,  
685 i.e., delta  $z = 0.02$ . The impact is greater for CO<sub>2</sub> rather than for CH<sub>4</sub>, whose gaseous  
686 behaviour is closer to ideal conditions. Even at this moderate pressure (10 bar),  
687 neglecting deviations from ideal gas behaviour can lead to inaccuracies in the system  
688 model. For example, at 50 bar and 25 °C, the delta  $z$  for CO<sub>2</sub> is 0.68, indicating that  
689 32% of the value calculated for the bulk gas CO<sub>2</sub> would be incorrect if ideal gas  
690 assumptions were used. Due to the exothermic nature of the adsorption process, the  
691 temperature can increase by up to 100 °C during the latter part of the adsorption step, <sup>[59]</sup>  
692 but the largest deviations from ideal gas assumptions occur at low temperatures.

693           • Temperature dependence

694 The main difference between the models is whether local thermal equilibrium  
 695 (LTE) <sup>[86, 89, 95]</sup> is assumed or not (No LTE). <sup>[59, 68, 90, 91, 96, 97]</sup> LTE assumes that the gas  
 696 and the solid adsorbent temperatures are equal at all points and all times.

697 Assuming that the process is isothermal greatly simplifies the design equations. It  
 698 eliminates the need for heat balance equations, and removes temperature dependencies  
 699 for physical properties, fluid velocities and adsorption equilibria. <sup>[72]</sup> Except when the  
 700 concentration of the adsorbable component is low and the heat of adsorption is small,  
 701 which is not the case for CO<sub>2</sub>/CH<sub>4</sub> separation, it is often difficult to obtain a very good  
 702 approximation of isothermal operation, even in a small column. <sup>[40]</sup> The model of an  
 703 isothermal particle in which all resistance to mass transfer is due to intraparticle  
 704 diffusion, while resistance to heat transfer is confined to the external film, therefore  
 705 appears to be a realistic representation for most conditions of practical importance. <sup>[40]</sup>

706 The temperature evolution of the PSA system is obtained by applying an energy  
 707 balance in the packed-bed column. PSA processes involve cyclic adsorption and  
 708 desorption, which are exothermic and endothermic, respectively. The energy balance is  
 709 the rate of change in internal energy of a packed bed element and adsorbent particle  
 710 over time  $t$ . Thus, when the process is not considered to be isothermal (no local thermal  
 711 equilibrium), the heat balance of the fluid phase and the heat transfer rate can be  
 712 expressed respectively as follows: <sup>[74]</sup>

$$\frac{\partial T_f}{\partial t} + v \frac{dT_f}{dZ} + \frac{c_s}{c_f} \frac{1 - \varepsilon}{\varepsilon} \frac{\partial T_s}{\partial t} + \frac{\Delta H}{c_f} \frac{1 - \varepsilon}{\varepsilon} \frac{\partial \bar{q}_l}{\partial t} = 0 \quad (15)$$

$$\frac{\partial T_s}{\partial t} = ha(T_f - T_s) - \frac{\Delta H}{c_s} \frac{\partial \bar{q}_l}{\partial t} \quad (16)$$

713 where  $T_f$  is the fluid temperature,  $v$  is the gas superficial velocity,  $Z$  is the axial position  
 714 along the column,  $\varepsilon$  is the bed porosity,  $T_s$  is the solid temperature,  $c_s$  is the specific heat  
 715 capacity of the solid,  $c_f$  is the specific heat capacity of the fluid,  $\Delta H$  is the heat of

716 adsorption,  $\bar{q}_i$  is the average concentration of adsorbed component  $i$ ,  $h$  is the heat  
717 transfer coefficient between fluid and particle and  $a$  is specific surface area available for  
718 heat transfer.

719 • Momentum balance

720 The momentum balance accounts for the forces acting on the fluid as it flows  
721 through the packed bed, which include friction between the fluid and the particle  
722 surface, as well as resistance caused by bed geometry and voids. This resistance results  
723 in a pressure drop, which depends on particle size, fluid velocity and bed dimensions.  
724 <sup>[72]</sup> Pressure drop  $\partial P/\partial Z$  in the column is generally modelled using the hydrodynamics  
725 of flow in porous media. This is usually described by the Ergun equation, which  
726 accounts for non-linear and turbulent flows: <sup>[74]</sup>

$$\frac{\partial P}{\partial Z} = 3.5 + 300 \left( \frac{1 - \varepsilon}{Re} \right) \left( \frac{1 - \varepsilon}{\varepsilon^3} \right) \frac{\dot{m}^2}{2d_p \rho} \quad (17)$$

727 where  $Re$  is the Reynold number,  $\dot{m}$  is the mass flow rate,  $d_p$  is particle diameter and  $\rho$   
728 is the fluid density.

729 • Numerical solution

730 The resulting mathematical model consists of a set of partial differential equations  
731 (PDEs), which exhibit steep fronts and non-linear behaviour,<sup>[99]</sup> presenting sharp  
732 changes in solution values that are difficult to predict accurately in numerical  
733 simulation. This complex system of mathematical equations is usually solved by  
734 commercial software such as Aspen<sup>[90–92]</sup> and gPROMS,<sup>[59, 68, 95–97]</sup> which incorporate  
735 numerical solution techniques for spatial discretization methods such as finite  
736 differences<sup>[59, 95, 96]</sup> or orthogonal collocation.<sup>[68, 86, 97]</sup> Finite-difference techniques <sup>[100]</sup>  
737 involve discretization of the spatial and time domain to convert PDEs into a set of linear  
738 and nonlinear algebraic equations, which can then be solved by Gaussian elimination  
739 for linear algebraic equations and Newton's method for nonlinear algebraic equations.



740 <sup>[40]</sup> The orthogonal collocation method approximates the solution using a set of basic  
741 functions, such as polynomials, evaluated at specific collocation points. This method  
742 differs from finite difference methods in that the solution is represented as a continuous  
743 or piecewise continuous function.<sup>[101]</sup> The orthogonal collocation method significantly  
744 reduces the number of discretized equations due to the lower number of internal points,  
745 resulting in rapid convergence.<sup>[89]</sup> One of the limitations of these methods is that solving  
746 the large set of PDEs does not ensure a real-valued solution, and the Newton solver may  
747 fail when confronted with the steep fronts that are typical of PSA separation.<sup>[99]</sup>

748 One of the normal shortcomings of the simulation process is the difficulty of  
749 achieving cycle steady state (CSS), which depends on the convergence towards  
750 consistent values of performance indicators such as CH<sub>4</sub> purity and recovery. Generally  
751 speaking, performance indicators should not vary by more than 1% or, in the most  
752 stringent cases, 0.1%. PSA cycles involving additional steps such as the inclusion of  
753 pressure equalizers or more than one adsorbent layer in the bed may pose more  
754 difficulties in achieving CSS, as there are more interactions, non-linear behaviours and  
755 more extensive range of system conditions. A basic Skarstrom cycle with a zeolite as  
756 adsorbent was reported to reach CSS after only 5 cycles,<sup>[86]</sup> on the other hand, PSA  
757 cycles with pressure equalization reach CSS after 70 cycles for a zeolite.<sup>[59, 96]</sup> Examples  
758 of acceleration schemes for CSS iterations are extrapolators in the quasi-linear  
759 convergence region and the recursive projection method of Shroff and Keller.<sup>[99]</sup>

760 Achieving CSS is important for correctly evaluating the performance of a PSA  
761 process, which is essential for optimizing its operating conditions and design  
762 parameters. The optimization process can be based on adjusting or improving  
763 parameters such as maximizing CH<sub>4</sub> recovery and purity, or reducing energy  
764 consumption for a desired CH<sub>4</sub> purity, for instance. The variables modified are normally

765 cycle design, operating conditions and adsorbent properties. The literature describes  
766 some optimization methods for PSA systems.<sup>[99, 102-104]</sup> In the context of CO<sub>2</sub>/CH<sub>4</sub>  
767 separation, the Response Surface Methodology (RSM) was investigated to achieve  
768 maximum CH<sub>4</sub> purity and recovery with MOF UiO-66 as adsorbent.<sup>[91]</sup> The results  
769 showed that the UiO-66 adsorbent achieved optimized CH<sub>4</sub> purity of 99.99%, recovery  
770 of 99.99% and productivity of 8.57 mol kg<sup>-1</sup> h<sup>-1</sup> by varying the operating temperature  
771 and bed length/diameter ratio. In another study, a full factorial design method and  
772 analysis of variance (ANOVA) test were used to investigate the effects of various  
773 factors on CH<sub>4</sub> purity and recovery.<sup>[75]</sup> All factors were shown to significantly influence  
774 purity, with purge pressure being the most significant factor, followed by vacuum level.  
775 For CH<sub>4</sub> recovery, the ANOVA test revealed that feed pressure and adsorption stage  
776 duration were the most significant factors, while purge stage duration and vacuum level  
777 had less effect.

778 An optimization method was proposed to maximize CH<sub>4</sub> recovery while maintaining  
779 a specified CH<sub>4</sub> purity of 99% by adjusting the CH<sub>4</sub> composition in the feed gas.<sup>[105]</sup>  
780 The Sequential Quadratic Programming Descent solver was chosen due to its ability to  
781 handle discrete changes in boundaries and equations. The conclusion drawn from the  
782 analysis of the impact of feed gas composition is that increasing the CH<sub>4</sub> content in the  
783 feed gas improves CH<sub>4</sub> recovery. This result is logical, as a higher CH<sub>4</sub> content  
784 simplifies the PSA process, reducing the volume of CO<sub>2</sub> that needs to be separated and  
785 purged. This efficiency can reduce energy consumption and improve overall process  
786 economics.

787 **4.3 PSA Performance Evaluation**

788 **Tables 5, 6 and 7** provide information on various operating parameters for different  
789 PSA units that have been reported in the literature. **Table 5** focuses specifically on data  
790 from single-column studies. Conversely, **Tables 6 and 7** present information related to  
791 multi-column systems, where **Table 5** shows experimental data, and **Table 6** presents  
792 simulation results.

793 **[Table 5 here]**

794 **[Table 6 here]**

795 **[Table 7 here]**

796 Concerning the performance of the process, **Figure 7** shows purity-recovery-  
797 productivity-energy consumption plots for CO<sub>2</sub>/CH<sub>4</sub> separation by EVSA and VSA. In  
798 general, the literature presents numerous examples of processes demonstrating a trade-  
799 off between higher purity and lower recovery, or vice versa. In this work, the data  
800 presented from each study were based on the authors' own criteria to select the best  
801 result with the aim of achieving the optimum balance between recovery and purity, with  
802 an emphasis on purities above 95%.

803 The presented operating parameters include cycle type, cycle steps, type of adsorbent  
804 used, CO<sub>2</sub>/CH<sub>4</sub> feed gas ratio,  $P_a$  and  $P_d$ , CH<sub>4</sub> purity and recovery percentages,  
805 productivity in terms of mol<sub>CH<sub>4</sub></sub> kg<sup>-1</sup> h<sup>-1</sup>, and energy consumption in kWh mol<sub>CH<sub>4</sub></sub><sup>-1</sup>.  
806 Using mass balances that consider the gas feed to the PSA system, as well as the  
807 separation of CO<sub>2</sub> and CH<sub>4</sub> in the production, purge, and blowdown streams, we  
808 conducted calculations to assess the productivity and energy consumption of various  
809 studies based on the provided data. For the calculation of the biogas compression stage

810 to reach the feed or adsorption pressure in the PSA (Eq. 10), we assumed that the gas  
811 would be available at a pressure of 1 bar, as biogas is usually produced at close to  
812 atmospheric pressure from a biogas digester. In addition, the blowdown process was  
813 assumed to start at atmospheric pressure and proceed down to the desired sub-  
814 atmospheric pressure. Furthermore, in cases where precise information regarding the  
815 quantity of raffinate used to purge the columns was not available, it was assumed that  
816 10% of the overall production was allocated for this purpose.

817 The results of the studies are representative of real-world scenarios where the CO<sub>2</sub>  
818 content in the feed gas stream can vary from around 20 to 50%. At the laboratory scale,  
819 the design of PSA units is highly adaptable, allowing the use of single-column  
820 configurations,<sup>[68, 106–109]</sup> as presented in **Table 5**. However, the use of a single column  
821 in the cycle is not an accurate representation of the actual PSA process, as it cannot be  
822 continuously fed and sometimes requires purging with pure CH<sub>4</sub>.<sup>[59]</sup> Although it can still  
823 serve as a valuable tool for validating numerical models of the PSA process and provide  
824 valuable data for exploring alternative cycles, on an industrial scale, the PSA unit  
825 comprises multiple columns operating in parallel, including configurations with two,  
826 three or more columns. Apart from the fact that the gas feed is not continuous, a single  
827 column does not allow incorporation of the pressure equalization step, which was the  
828 first improvement to the original Skarstrom's cycle introduced by Berlin in 1967.<sup>[40, 110]</sup>  
829 This pressure equalization step can indeed significantly improve CH<sub>4</sub> recovery.

830 Generally, the most commonly used adsorbent to capture CO<sub>2</sub> in PSA units is either  
831 a CMS,<sup>[79, 111, 112]</sup> for which it is worth recalling that its selectivity is mainly driven by  
832 kinetic factors, or a zeolite,<sup>[39, 59, 75, 79]</sup> whose selectivity is mainly determined by both  
833 thermodynamic equilibrium and kinetic aspects. Although ACs and MOFs<sup>[68]</sup> are  
834 potential adsorbents, they are less frequently used due to their lower selectivity and

835 relatively recent stage of development, as well as high production cost, respectively.  
836 While MOFs offer promising opportunities for CO<sub>2</sub> capture, exhibiting higher CO<sub>2</sub>/CH<sub>4</sub>  
837 selectivity and PSA working capacity ratio, further research is necessary to fully explore  
838 their potential in this application.

839 The sub-atmospheric blowdown regeneration method is widely used in most cycles,  
840 indicating that adsorbed CO<sub>2</sub> cannot be easily regenerated by simple atmospheric  
841 depressurization. However, in the only experimental multi-column example where the  
842 columns were regenerated at atmospheric pressure,<sup>[111]</sup> a low CH<sub>4</sub> recovery of 71 % was  
843 achieved, resulting in relatively low productivity. This low recovery can be attributed to  
844 a high amount of CH<sub>4</sub> that is part of the raffinate produced and used in the regeneration  
845 process as purge. Similarly, the two single-bed studies that used atmospheric pressure  
846 depressurization also resulted in very low recoveries and productivities.<sup>[68, 108]</sup> Although  
847 atmospheric depressurization results in low energy consumption due to the absence of a  
848 vacuum pump, the normalized energy consumption per amount of CH<sub>4</sub> produced is  
849 higher than in many VSA or EVSA studies.

850 **[Figure 7 here]**

851 The introduction of pressure equalization (see **Figure 7a**) in the VSA cycle (see  
852 **Figure 7b**) offers significant improvements in recovery, productivity and energy  
853 consumption.<sup>[33, 68, 87, 112, 113, 120]</sup> For instance, in an EVSA cycle, the optimal PSA-  
854 adsorbent configuration (see green line in **Figure 7a**) achieved a productivity of 15.6  
855 mol<sub>CH<sub>4</sub></sub> kg<sup>-1</sup> h<sup>-1</sup> with an energy consumption of 0.0039 kWh mol<sub>CH<sub>4</sub></sub><sup>-1</sup>.<sup>[79]</sup> Conversely, in  
856 the VSA cycle, the most favorable scenario (see green line in **Figure 7b**) achieved a  
857 productivity of 12.8 mol<sub>CH<sub>4</sub></sub> kg<sup>-1</sup> h<sup>-1</sup> and an energy consumption of 0.0044 kWh mol<sub>CH<sub>4</sub></sub><sup>-1</sup>  
858 <sup>1</sup>.<sup>[39]</sup>

859 Recovery is improved by ensuring that the adsorption and desorption phases are  
860 carried out evenly across all the adsorbent beds, ensuring full utilization of the beds and  
861 maximizing the recovery of the target component. Without pressure equalization, gas  
862 flow may be unevenly distributed across the adsorbent beds, leading to preferential  
863 adsorption and desorption in certain sections of the beds. Moreover, by equalizing the  
864 pressure between the two adsorption columns, the energy derived from the compressed  
865 gas in the high-pressure bed is used to partially pressurize the low-pressure bed. Due to  
866 the partial depletion of the strongly adsorbed species in this gas, the work of separation  
867 is conserved, resulting in energy savings. This process effectively reduces blowdown  
868 losses by about 50%, thus enhancing the recovery of the raffinate product.<sup>[40]</sup>  
869 Additionally, maximizing the recovery of CH<sub>4</sub> is of highest importance due to its  
870 greenhouse effect, which is even more potent than that of CO<sub>2</sub> and contributes to global  
871 warming. It is indeed remarkable that the warming potential of CH<sub>4</sub> is 21 times greater  
872 than that of CO<sub>2</sub>.<sup>[59]</sup>

873 Typically, the duration of a 2-bed adsorption cycle ranges between 150 s to 400 s.<sup>[38,</sup>  
874 <sup>39, 75, 79, 86]</sup> However, for scenarios involving more than two beds, additional tanks, or  
875 simulations of industrial scale systems,<sup>[68, 93, 112]</sup> the cycle time can increase  
876 significantly, exceeding 1000 s. The duration of the cycle should be sufficient to ensure  
877 effective gas adsorption when using adsorbents with high equilibrium adsorption  
878 capacity, while fast-adsorbing adsorbents require a shorter cycle time to facilitate fast  
879 kinetic adsorption.

880 Optimum productivity was achieved by maintaining low adsorption pressures,  
881 specifically 2 atm or less.<sup>[39, 79]</sup> Notably, the most effective desorption pressure for  
882 regenerating the bed was 0.1 atm. Although such a minimal desorption pressure requires  
883 considerable energy consumption on the part of the vacuum pump, this approach

884 demonstrates low energy consumption per mole of CH<sub>4</sub> produced. In other words,  
885 despite the high energy requirements, the substantial CH<sub>4</sub> production outweighs the  
886 energy consumption, making this operational method advantageous. An effective way  
887 to further improve the system and reduce energy consumption is to reduce  $P_a$  or  
888 increase the sub-atmospheric  $P_d$ , which is usually 0.1 atm. Increasing  $P_d$  to 0.2 or 0.3  
889 atm could result in significant savings.

890 Remarkably, different performances can be achieved within the same family of  
891 materials, even if the corresponding materials exhibit similar selectivity and PSA  
892 working capacity ratio properties. For instance, NaUSY zeolite,<sup>[79]</sup> which demonstrated  
893 the highest productivity and lowest energy consumption (see the green line “best” in  
894 **Figure 7a**), was used in a purge-free EVSA cycle and exhibited a selectivity and PSA  
895 working capacity ratio of 50 and 30, respectively. In contrast, zeolite 13X<sup>[59]</sup> was  
896 employed in an EVSA cycle with purge and exhibited a selectivity and PSA working  
897 capacity ratio of 58 and 26, respectively. Both cycles achieved purities in excess of  
898 99%, but the EVSA cycle without purge resulted in more than doubling the productivity  
899 and a reduction in energy consumption to less than half. Consequently, it would be  
900 advantageous to eliminate purging by regenerating the bed at very low vacuum pressure  
901 (0.1 atm).

902 The performance evaluation of the MOF MIL-53<sup>[68]</sup> as an adsorbent for CO<sub>2</sub>/CH<sub>4</sub>  
903 separation differs from other cases because the objective is to produce both CH<sub>4</sub> and  
904 CO<sub>2</sub> at high purity. It has been found that achieving these levels of purity and recovery  
905 comes at the expense of high energy consumption. This high energy consumption arises  
906 from the fact that an additional step is required to pressurize and adsorb the effluent  
907 from column regeneration. Moreover, the productivity in terms of CH<sub>4</sub> production was  
908 observed to be very low (2.1 mol<sub>CH<sub>4</sub></sub> kg<sup>-1</sup> h<sup>-1</sup>). This low productivity could be attributed

909 to the adsorbent's low CO<sub>2</sub>/CH<sub>4</sub> selectivity of 4 at 4 bar, which is significantly lower  
910 than the selectivity of zeolites, typically around 50. Nevertheless, a new process  
911 configuration has been proposed, <sup>[115]</sup> using zeolite 5A with two PSA units, each  
912 containing four beds. In this setup, the second unit processes the off-gas from the first  
913 unit, which has separated the CO<sub>2</sub> from the residual gas stream. The residual stream is  
914 then recycled back to the first unit, improving CH<sub>4</sub> recovery. Final results showed CH<sub>4</sub>  
915 purity and recovery of 99.4% and 99.0%, respectively, with modest energy consumption  
916 of 0.0056 kWh mol<sub>CH<sub>4</sub></sub><sup>-1</sup> and productivity of 8.2 mol<sub>CH<sub>4</sub></sub> kg<sup>-1</sup> h<sup>-1</sup>. In addition, the system  
917 produced CO<sub>2</sub> with a purity of 99.1%. This process represents a promising alternative  
918 for achieving high CH<sub>4</sub> recovery and purity, while also producing high-purity CO<sub>2</sub>.

919 CMSs enable faster diffusion of CO<sub>2</sub>, reducing adsorption time and increasing  
920 productivity. However, CMSs have a significantly lower PSA working capacity ratio  
921 than zeolites. Furthermore, the use of CMSs involves the utilization of only a fraction of  
922 the overall equilibrium capacity, leading to a reduction in productivity.<sup>[109]</sup> Zeolites  
923 possess steeper isotherms and high CO<sub>2</sub> adsorption enthalpy, necessitating high vacuum  
924 conditions for bed regeneration. Conversely, CO<sub>2</sub> isotherms in CMSs are less steep,  
925 allowing vacuum desorption at relatively higher pressures.<sup>[38]</sup> Although column  
926 regeneration at atmospheric pressure has been achieved for CMSs,<sup>[111]</sup> it resulted in  
927 lower recovery and productivity. Despite this, CMS regeneration has been carried out at  
928 low vacuum pressures of 0.1-0.3 atm.<sup>[87, 109, 120]</sup> Among these processes, the EVSA  
929 process without purge<sup>[79]</sup> stands out as the most optimal for CMS, offering a  
930 productivity of 11.3 mol<sub>CH<sub>4</sub></sub> kg<sup>-1</sup> h<sup>-1</sup>. This value is slightly lower than the productivity of  
931 the best zeolite system, which is 15.6 mol<sub>CH<sub>4</sub></sub> kg<sup>-1</sup> h<sup>-1</sup>, indicating that the higher working  
932 capacity ratio of PSA in zeolites may be more advantageous than the fast diffusion  
933 process of CMSs. Additionally, the energy consumption of the two systems is similar,



934 0.0038 and 0.0039 kWh mol<sub>CH<sub>4</sub></sub><sup>-1</sup>, respectively. Overall, CMSs can offer comparable  
935 performance to zeolites. To address the issue of low utilization of equilibrium capacity  
936 in kinetic-selective adsorbents, Grande and Rodrigues<sup>[38]</sup> introduced a mixed layer of  
937 CMS and zeolite at the end of the column. By implementing this approach, they were  
938 able to achieve a substantial increase in productivity compared with a process relying  
939 solely on CMSs as adsorbent. This improvement was mainly attributed to the ability to  
940 process a larger amount of feed, as the column retained more CO<sub>2</sub> while retaining the  
941 same dimensions.

942 Most studies do not consider the use of ACs, due to their perceived lack of CO<sub>2</sub>/CH<sub>4</sub>  
943 selectivity. Nevertheless, these materials offer several potential advantages, including a  
944 reduced environmental impact and uncontrolled waste disposal, lower emissions during  
945 their production and the possibility of establishing a circular economy and achieving  
946 lower carbon emissions compared with other CO<sub>2</sub> capture methods.<sup>[108]</sup> Unfortunately,  
947 to our knowledge, there are no multi-column experimental studies on ACs.  
948 Furthermore, none of the AC producers offers a commercially available AC specifically  
949 designed for CO<sub>2</sub>/CH<sub>4</sub> gas separation.

950 To design an efficient adsorbent/pressure swing adsorption (PSA) system for gas  
951 separation, the first priority is to select a material with high CO<sub>2</sub>/CH<sub>4</sub> selectivity.  
952 Ideally, selectivity should be over 50 at a pressure of 1 bar, unless the material operates  
953 on a kinetic basis, such as CMS. The PSA working capacity ratio, based on expected  
954 operating pressures, should ideally also be greater than 50. When tested in lab-scale  
955 PSA systems, at the desired CH<sub>4</sub> purity, productivity in excess of 8 mol<sub>CH<sub>4</sub></sub> kg<sup>-1</sup> h<sup>-1</sup> is  
956 generally acceptable, with the best-performing systems in the literature reporting values  
957 above 11 mol<sub>CH<sub>4</sub></sub> kg<sup>-1</sup> h<sup>-1</sup>. In terms of energy efficiency, an energy consumption of  
958 0.0060 kWh mol<sup>-1</sup> CH<sub>4</sub> represents an upper limit for acceptable operation, while the

959 optimum range is typically between 0.0030 and 0.0040 kWh mol<sup>-1</sup> CH<sub>4</sub>. These  
960 benchmarks are essential to ensure that the PSA system is not only productive, but also  
961 energy-efficient, balancing both performance and sustainability.

## 962 **5. Conclusions**

963 In this comprehensive review, various adsorbents were compared based on their  
964 selectivity for CO<sub>2</sub>/CH<sub>4</sub> adsorption and their working capacity ratio in pressure swing  
965 adsorption (PSA) for biogas upgrading. Zeolites exhibit significantly higher equilibrium  
966 selectivity, making them favorable for PSA units. While metal-organic frameworks  
967 (MOFs) may be an alternative, further research is needed for practical PSA application.  
968 Carbon molecular sieves (CMSs), despite lacking high equilibrium selectivity, are  
969 excellent PSA candidates due to exceptional kinetic selectivity, comparable to zeolites.  
970 Activated carbons (ACs), with lower selectivity, offer sustainability and cost-  
971 effectiveness. Despite extensive research, integrating results into real multi-column PSA  
972 systems is lacking. To foster global research efforts, the development of highly selective  
973 materials for CO<sub>2</sub> over CH<sub>4</sub> is crucial for global PSA process optimization.

974 The simulation of PSA systems was examined by comparing dynamic modeling  
975 from literature. All the studies utilize the axially dispersed plug flow model for  
976 describing fluid flow and they use the Multicomponent Langmuir isotherm and the  
977 Linear Driving Force model for equilibrium and mass transfer kinetics. Ideal gas  
978 behavior is assumed, although deviations at high pressures are accounted with equations  
979 of state. Achieving cycle steady state is essential for evaluating PSA performance, with  
980 optimization methods often focusing on maximizing CH<sub>4</sub> recovery and purity or  
981 reducing energy consumption.

982 A comparative analysis of PSA unit operations was conducted, integrating various  
983 performance parameters such as purity, recovery, productivity, and energy  
984 consumption. The study revealed that, while obtaining high-purity CH<sub>4</sub> was relatively  
985 straightforward using various adsorbents or cycles, it is crucial to consider productivity  
986 and energy consumption, as these factors have a direct impact on the competitiveness  
987 and sustainability of the process. According to these results, we can assert that the most  
988 optimal approach for achieving high purity and productivity with low energy  
989 consumption is the cycle involving pressure equalization and sub-atmospheric  
990 regeneration with either zeolites or CMSs.

## 991 **6. Funding details**

992 This research was funded by the French National Research Agency (ANR) through  
993 the "CarBioLab" project, as part of the LabCom "Joint Laboratories" program, 2021  
994 edition. This work has also been partially supported by project no ANR-22-PESP-0007,  
995 CATALPA project as part of the PEPR SPLEEN, from the French National Research  
996 Agency (ANR) (France 2030).

## 997 **7. Disclosure statement**

998 The authors report there are no competing interests to declare.

## 999 **8. References**

- 1000 [1] Chen, X. Y.; Vinh-Thang, H.; Ramirez, A. A.; Rodrigue, D.; Kaliaguine, S.  
1001 Membrane Gas Separation Technologies for Biogas Upgrading. *RSC Adv.*, **2015**, *5*  
1002 (31), 24399–24448. <https://doi.org/10.1039/C5RA00666J>.  
1003 [2] Abd, A. A.; Othman, M. R.; Shabbani, H. J. K.; Helwani, Z. Biomethane  
1004 Upgrading to Transportation Fuel Quality Using Spent Coffee for Carbon Dioxide  
1005 Capture in Pressure Swing Adsorption. *Journal of Environmental Chemical*  
1006 *Engineering*, **2022**, *10* (2), 107169. <https://doi.org/10.1016/j.jece.2022.107169>.

- 1007 [3] Zhang, Y.; Zhang, P.; Yu, W.; Wang, J.; Deng, Q.; Yang, J.; Zeng, Z.; Xu, M.;  
1008 Deng, S. Facile and Controllable Preparation of Ultramicroporous Biomass-  
1009 Derived Carbons and Application on Selective Adsorption of Gas-Mixtures. *Ind.*  
1010 *Eng. Chem. Res.*, **2018**, *57* (42), 14191–14201.  
1011 <https://doi.org/10.1021/acs.iecr.8b02139>.
- 1012 [4] Abd, A. A.; Naji, S. Z.; Hashim, A. S.; Othman, M. R. Carbon Dioxide Removal  
1013 through Physical Adsorption Using Carbonaceous and Non-Carbonaceous  
1014 Adsorbents: A Review. *Journal of Environmental Chemical Engineering*, **2020**, *8*  
1015 (5), 104142. <https://doi.org/10.1016/j.jece.2020.104142>.
- 1016 [5] Aghel, B.; Behaein, S.; Alobaid, F. CO<sub>2</sub> Capture from Biogas by Biomass-Based  
1017 Adsorbents: A Review. *Fuel*, **2022**, *328*, 125276.  
1018 <https://doi.org/10.1016/j.fuel.2022.125276>.
- 1019 [6] Bahrun, M. H. V.; Bono, A.; Othman, N.; Zaini, M. A. A. Carbon Dioxide  
1020 Removal from Biogas through Pressure Swing Adsorption – A Review. *Chemical*  
1021 *Engineering Research and Design*, **2022**, *183*, 285–306.  
1022 <https://doi.org/10.1016/j.cherd.2022.05.012>.
- 1023 [7] Abd, A. A.; Othman, M. R.; Naji, S. Z.; Hashim, A. S. Methane Enrichment in  
1024 Biogas Mixture Using Pressure Swing Adsorption: Process Fundamental and  
1025 Design Parameters. *Materials Today Sustainability*, **2021**, *11–12*, 100063.  
1026 <https://doi.org/10.1016/j.mtsust.2021.100063>.
- 1027 [8] Shah, G.; Ahmad, E.; Pant, K. K.; Vijay, V. K. Comprehending the Contemporary  
1028 State of Art in Biogas Enrichment and CO<sub>2</sub> Capture Technologies via Swing  
1029 Adsorption. *International Journal of Hydrogen Energy*, **2021**, *46* (9), 6588–6612.  
1030 <https://doi.org/10.1016/j.ijhydene.2020.11.116>.
- 1031 [9] Grande, C. A. Biogas Upgrading by Pressure Swing Adsorption. In *Biofuel's*  
1032 *Engineering Process Technology*; 2011.
- 1033 [10] Hosseini, S. S.; Denayer, J. F. M. Biogas Upgrading by Adsorption Processes:  
1034 Mathematical Modeling, Simulation and Optimization Approach – A Review.  
1035 *Journal of Environmental Chemical Engineering*, **2022**, *10* (3), 107483.  
1036 <https://doi.org/10.1016/j.jece.2022.107483>.
- 1037 [11] INTERNATIONAL ENERGY AGENCY. *Key World Energy Statistics 2021*;  
1038 *Statistics*; 2021; p 6.
- 1039 [12] A European Green Deal [https://commission.europa.eu/strategy-and-](https://commission.europa.eu/strategy-and-policy/priorities-2019-2024/european-green-deal_en)  
1040 [policy/priorities-2019-2024/european-green-deal\\_en](https://commission.europa.eu/strategy-and-policy/priorities-2019-2024/european-green-deal_en) (accessed Dec 13, 2022).
- 1041 [13] How much energy in biogas Inoplex [https://inoplex.com.au/information/how-](https://inoplex.com.au/information/how-much-energy-is-in-biogas/)  
1042 [much-energy-is-in-biogas/](https://inoplex.com.au/information/how-much-energy-is-in-biogas/) (accessed Dec 13, 2022).
- 1043 [14] Seo, D.-J.; Gou, Z.; Fujita, H.; Fujii, T.; Sakoda, A. Simple Fabrication of  
1044 Molecular Sieving Carbon for Biogas Upgrading via a Temperature Controlled  
1045 Carbonization of *Phyllostachys Pubescens*. *Renewable Energy*, **2016**, *86*, 693–702.  
1046 <https://doi.org/10.1016/j.renene.2015.09.006>.
- 1047 [15] Sheng, K.; Chen, X.; Pan, J.; Kloss, R.; Wei, Y.; Ying, Y. Effect of Ammonia and  
1048 Nitrate on Biogas Production from Food Waste via Anaerobic Digestion.  
1049 *Biosystems Engineering*, **2013**, *116* (2), 205–212.  
1050 <https://doi.org/10.1016/j.biosystemseng.2013.08.005>.
- 1051 [16] Nyamukamba, P.; Mukumba, P.; Chikukwa, E. S.; Makaka, G. Biogas Upgrading  
1052 Approaches with Special Focus on Siloxane Removal—A Review. *Energies*,  
1053 **2020**, *13* (22), 6088. <https://doi.org/10.3390/en13226088>.
- 1054 [17] Wang, X.; Wang, D.; Song, M.; Xin, C.; Zeng, W. Tetraethylenepentamine-  
1055 Modified Activated Semicoke for CO<sub>2</sub> Capture from Flue Gas. *Energy Fuels*,  
1056 **2017**, *31* (3), 3055–3061. <https://doi.org/10.1021/acs.energyfuels.6b03177>.

- 1057 [18] Irani, M.; Jacobson, A. T.; Gasem, K. A. M.; Fan, M. Modified Carbon  
 1058 Nanotubes/Tetraethylenepentamine for CO<sub>2</sub> Capture. *Fuel*, **2017**, *206*, 10–18.  
 1059 <https://doi.org/10.1016/j.fuel.2017.05.087>.
- 1060 [19] Liu, Y.; Lin, X.; Wu, X.; Liu, M.; Shi, R.; Yu, X. Pentaethylenhexamine Loaded  
 1061 SBA-16 for CO<sub>2</sub> Capture from Simulated Flue Gas. *Powder Technology*, **2017**,  
 1062 *318*, 186–192. <https://doi.org/10.1016/j.powtec.2017.06.002>.
- 1063 [20] Kadam, R.; Panwar, N. L. Recent Advancement in Biogas Enrichment and Its  
 1064 Applications. *Renewable and Sustainable Energy Reviews*, **2017**, *73*, 892–903.  
 1065 <https://doi.org/10.1016/j.rser.2017.01.167>.
- 1066 [21] Kabeyi, M. J. B.; Olanrewaju, O. A. Technologies for Biogas to Electricity  
 1067 Conversion. *Energy Reports*, **2022**, *8*, 774–786.  
 1068 <https://doi.org/10.1016/j.egyr.2022.11.007>.
- 1069 [22] Khan, M. U.; Lee, J. T. E.; Bashir, M. A.; Dissanayake, P. D.; Ok, Y. S.; Tong, Y.  
 1070 W.; Shariati, M. A.; Wu, S.; Ahring, B. K. Current Status of Biogas Upgrading for  
 1071 Direct Biomethane Use: A Review. *Renewable and Sustainable Energy Reviews*,  
 1072 **2021**, *149*, 111343. <https://doi.org/10.1016/j.rser.2021.111343>.
- 1073 [23] Angelidaki, I.; Treu, L.; Tsapekos, P.; Luo, G.; Campanaro, S.; Wenzel, H.;  
 1074 Kougiass, P. G. Biogas Upgrading and Utilization: Current Status and Perspectives.  
 1075 *Biotechnology Advances*, **2018**, *36* (2), 452–466.  
 1076 <https://doi.org/10.1016/j.biotechadv.2018.01.011>.
- 1077 [24] Yuan, B.; Wang, J.; Chen, Y.; Wu, X.; Luo, H.; Deng, S. Unprecedented  
 1078 Performance of N-Doped Activated Hydrothermal Carbon towards C<sub>2</sub>H<sub>6</sub>/CH<sub>4</sub>,  
 1079 CO<sub>2</sub>/CH<sub>4</sub>, and CO<sub>2</sub>/H<sub>2</sub> Separation. *J. Mater. Chem. A*, **2016**, *4* (6), 2263–2276.  
 1080 <https://doi.org/10.1039/C5TA08436A>.
- 1081 [25] Song, C.; Liu, Q.; Deng, S.; Li, H.; Kitamura, Y. Cryogenic-Based CO<sub>2</sub> Capture  
 1082 Technologies: State-of-the-Art Developments and Current Challenges. *Renewable  
 1083 and Sustainable Energy Reviews*, **2019**, *101*, 265–278.  
 1084 <https://doi.org/10.1016/j.rser.2018.11.018>.
- 1085 [26] Baena-Moreno, F. M.; le Saché, E.; Pastor-Pérez, L.; Reina, T. R. Membrane-  
 1086 Based Technologies for Biogas Upgrading: A Review. *Environ Chem Lett*, **2020**,  
 1087 *18* (5), 1649–1658. <https://doi.org/10.1007/s10311-020-01036-3>.
- 1088 [27] Bagreev, A.; Badosz, T. J. A Role of Sodium Hydroxide in the Process of  
 1089 Hydrogen Sulfide Adsorption/Oxidation on Caustic-Impregnated Activated  
 1090 Carbons. *Ind. Eng. Chem. Res.*, **2002**, *41* (4), 672–679.  
 1091 <https://doi.org/10.1021/ie010599r>.
- 1092 [28] Guo, J.; Luo, Y.; Lua, A. C.; Chi, R.; Chen, Y.; Bao, X.; Xiang, S. Adsorption of  
 1093 Hydrogen Sulphide (H<sub>2</sub>S) by Activated Carbons Derived from Oil-Palm Shell.  
 1094 *Carbon*, **2007**, *45* (2), 330–336. <https://doi.org/10.1016/j.carbon.2006.09.016>.
- 1095 [29] Yan, R.; Liang, D. T.; Tsen, L.; Tay, J. H. Kinetics and Mechanisms of H<sub>2</sub>S  
 1096 Adsorption by Alkaline Activated Carbon. *Environ. Sci. Technol.*, **2002**, *36* (20),  
 1097 4460–4466. <https://doi.org/10.1021/es0205840>.
- 1098 [30] Sigot, L.; Ducom, G.; Benadda, B.; Labouré, C. Comparison of Adsorbents for H<sub>2</sub>  
 1099 S and D<sub>4</sub> Removal for Biogas Conversion in a Solid Oxide Fuel Cell.  
 1100 *Environmental Technology*, **2016**, *37* (1), 86–95.  
 1101 <https://doi.org/10.1080/09593330.2015.1063707>.
- 1102 [31] Cruz, A. J.; Pires, J.; Carvalho, A. P.; De Carvalho, M. B. Physical Adsorption of  
 1103 H<sub>2</sub>S Related to the Conservation of Works of Art: The Role of the Pore Structure  
 1104 at Low Relative Pressure. *Adsorption*, **2005**, *11* (5–6), 569–576.  
 1105 <https://doi.org/10.1007/s10450-005-5614-3>.

- 1106 [32] Bak, C.; Lim, C.-J.; Kim, Y.-D.; Kim, W.-S. Multi-Stage Adsorptive Purification  
 1107 Process for Improving Desulfurization Performance of Biogas. *Separation and*  
 1108 *Purification Technology*, **2019**, *227*, 115702.  
 1109 <https://doi.org/10.1016/j.seppur.2019.115702>.
- 1110 [33] Gong, H.; Chen, Z.; Fan, Y.; Zhang, M.; Wu, W.; Wang, W. Surface Modification  
 1111 of Activated Carbon for Siloxane Adsorption. *Renewable Energy*, **2015**, *83*, 144–  
 1112 150. <https://doi.org/10.1016/j.renene.2015.04.004>.
- 1113 [34] Tran, V. T. L.; Gélin, P.; Ferronato, C.; Mascunan, P.; Rac, V.; Chovelon, J.-M.;  
 1114 Postole, G. Siloxane Adsorption on Activated Carbons: Role of the Surface  
 1115 Chemistry on Sorption Properties in Humid Atmosphere and Regenerability  
 1116 Issues. *Chemical Engineering Journal*, **2019**, *371*, 821–832.  
 1117 <https://doi.org/10.1016/j.cej.2019.04.087>.
- 1118 [35] Tran, V. T. L.; Gélin, P.; Ferronato, C.; Chovelon, J.; Fine, L.; Postole, G.  
 1119 Adsorption of Linear and Cyclic Siloxanes on Activated Carbons for Biogas  
 1120 Purification: Sorbents Regenerability. *Chemical Engineering Journal*, **2019**, *378*,  
 1121 122152. <https://doi.org/10.1016/j.cej.2019.122152>.
- 1122 [36] Álvarez-Gutiérrez, N.; Gil, M. V.; Rubiera, F.; Pevida, C. Adsorption Performance  
 1123 Indicators for the CO<sub>2</sub>/CH<sub>4</sub> Separation: Application to Biomass-Based Activated  
 1124 Carbons. *Fuel Processing Technology*, **2016**, *142*, 361–369.  
 1125 <https://doi.org/10.1016/j.fuproc.2015.10.038>.
- 1126 [37] Vilella, P. C.; Lira, J. A.; Azevedo, D. C. S.; Bastos-Neto, M.; Stefanutti, R.  
 1127 Preparation of Biomass-Based Activated Carbons and Their Evaluation for Biogas  
 1128 Upgrading Purposes. *Industrial Crops and Products*, **2017**, *109*, 134–140.  
 1129 <https://doi.org/10.1016/j.indcrop.2017.08.017>.
- 1130 [38] Grande, C. A.; Rodrigues, A. E. Layered Vacuum Pressure-Swing Adsorption for  
 1131 Biogas Upgrading. *Ind. Eng. Chem. Res.*, **2007**, *46* (23), 7844–7848.  
 1132 <https://doi.org/10.1021/ie070942d>.
- 1133 [39] Jiang, Y.; Ling, J.; Xiao, P.; He, Y.; Zhao, Q.; Chu, Z.; Liu, Y.; Li, Z.; Webley, P.  
 1134 A. Simultaneous Biogas Purification and CO<sub>2</sub> Capture by Vacuum Swing  
 1135 Adsorption Using Zeolite NaUSY. *Chemical Engineering Journal*, **2018**, *334*,  
 1136 2593–2602. <https://doi.org/10.1016/j.cej.2017.11.090>.
- 1137 [40] Ruthven, Douglas M; Farooq, Shamsuzzaman; Knaebel, Kent S. *Pressure Swing*  
 1138 *Adsorption*; VCH Publishers, Inc, 1994.
- 1139 [41] Boer, D. G.; Langerak, J.; Pescarmona, P. P. Zeolites as Selective Adsorbents for  
 1140 CO<sub>2</sub> Separation. *ACS Appl. Energy Mater.*, **2023**, *6* (5), 2634–2656.  
 1141 <https://doi.org/10.1021/acsaem.2c03605>.
- 1142 [42] Greco, G.; Canevesi, R. L. S.; Di Stasi, C.; Celzard, A.; Fierro, V.; Manyà, J. J.  
 1143 Biomass-Derived Carbons Physically Activated in One or Two Steps for  
 1144 CH<sub>4</sub>/CO<sub>2</sub> Separation. *Renewable Energy*, **2022**, *191*, 122–133.  
 1145 <https://doi.org/10.1016/j.renene.2022.04.035>.
- 1146 [43] Abd, A. A.; Othman, M. R.; Kim, J. A Review on Application of Activated  
 1147 Carbons for Carbon Dioxide Capture: Present Performance, Preparation, and  
 1148 Surface Modification for Further Improvement. *Environ Sci Pollut Res*, **2021**, *28*  
 1149 (32), 43329–43364. <https://doi.org/10.1007/s11356-021-15121-9>.
- 1150 [44] Abdeljaoued, A.; Querejeta, N.; Durán, I.; Álvarez-Gutiérrez, N.; Pevida, C.;  
 1151 Chahbani, M. Preparation and Evaluation of a Coconut Shell-Based Activated  
 1152 Carbon for CO<sub>2</sub>/CH<sub>4</sub> Separation. *Energies*, **2018**, *11* (7), 1748.  
 1153 <https://doi.org/10.3390/en11071748>.
- 1154 [45] Vivo-Vilches, J. F.; Pérez-Cadenas, A. F.; Maldonado-Hódar, F. J.; Carrasco-  
 1155 Marín, F.; Faria, R. P. V.; Ribeiro, A. M.; Ferreira, A. F. P.; Rodrigues, A. E.

- 1156 Biogas Upgrading by Selective Adsorption onto CO<sub>2</sub> Activated Carbon from  
 1157 Wood Pellets. *Journal of Environmental Chemical Engineering*, **2017**, 5 (2),  
 1158 1386–1393. <https://doi.org/10.1016/j.jece.2017.02.015>.
- 1159 [46] Surra, E.; Ribeiro, R. P. P. L.; Santos, T.; Bernardo, M.; Mota, J. P. B.; Lapa, N.;  
 1160 Esteves, I. A. A. C. Evaluation of Activated Carbons Produced from Maize Cob  
 1161 Waste for Adsorption-Based CO<sub>2</sub> Separation and Biogas Upgrading. *Journal of*  
 1162 *Environmental Chemical Engineering*, **2022**, 10 (1), 107065.  
 1163 <https://doi.org/10.1016/j.jece.2021.107065>.
- 1164 [47] Yang, H.; Gong, M.; Chen, Y. Preparation of Activated Carbons and Their  
 1165 Adsorption Properties for Greenhouse Gases: CH<sub>4</sub> and CO<sub>2</sub>. *Journal of Natural*  
 1166 *Gas Chemistry*, **2011**, 20 (5), 460–464. [https://doi.org/10.1016/S1003-](https://doi.org/10.1016/S1003-9953(10)60232-0)  
 1167 [9953\(10\)60232-0](https://doi.org/10.1016/S1003-9953(10)60232-0).
- 1168 [48] Munusamy, K.; Somani, R. S.; Bajaj, H. C. Breakthrough Adsorption Studies of  
 1169 Mixed Gases on Mango (*Mangifera Indica*L.) Seed Shell Derived Activated  
 1170 Carbon Extrudes. *Journal of Environmental Chemical Engineering*, **2015**, 3 (4),  
 1171 2750–2759. <https://doi.org/10.1016/j.jece.2015.05.010>.
- 1172 [49] Sun, Y.; Webley, P. A. Preparation of Activated Carbons with Large Specific  
 1173 Surface Areas from Biomass Corncob and Their Adsorption Equilibrium for  
 1174 Methane, Carbon Dioxide, Nitrogen, and Hydrogen. *Ind. Eng. Chem. Res.*, **2011**.
- 1175 [50] Rattanaphan, S.; Rungrotmongkol, T.; Kongsune, P. Biogas Improving by  
 1176 Adsorption of CO<sub>2</sub> on Modified Waste Tea Activated Carbon. *Renewable Energy*,  
 1177 **2020**, 145, 622–631. <https://doi.org/10.1016/j.renene.2019.05.104>.
- 1178 [51] Yang, F.; Wang, J.; Liu, L.; Zhang, P.; Yu, W.; Deng, Q.; Zeng, Z.; Deng, S.  
 1179 Synthesis of Porous Carbons with High N Content from Shrimp Shells for  
 1180 Efficient CO<sub>2</sub> Capture and Gas Separation.
- 1181 [52] Ahmadi, R.; Ardjmand, M.; Rashidi, A.; Rafizadeh, M. High Performance Novel  
 1182 Nano-adsorbents Derived - Natural Cellulose Fibers for Superior CO<sub>2</sub> Adsorption  
 1183 and CO<sub>2</sub> / CH<sub>4</sub> Separation. *Energy Sources, Part A: Recovery, Utilization, and*  
 1184 *Environmental Effects*, **2020**, 0 (0), 1–19.  
 1185 <https://doi.org/10.1080/15567036.2020.1845878>.
- 1186 [53] Li, Y.; Xu, R.; Wang, B.; Wei, J.; Wang, L.; Shen, M.; Yang, J. Enhanced N-  
 1187 Doped Porous Carbon Derived from KOH-Activated Waste Wool: A Promising  
 1188 Material for Selective Adsorption of CO<sub>2</sub>/CH<sub>4</sub> and CH<sub>4</sub>/N<sub>2</sub>. *Nanomaterials*,  
 1189 **2019**, 9 (2), 266. <https://doi.org/10.3390/nano9020266>.
- 1190 [54] Saadi, W.; Rodríguez-Sánchez, S.; Ruiz, B.; Najjar-Souissi, S.; Ouederni, A.;  
 1191 Fuente, E. From Pomegranate Peels Waste to One-Step Alkaline Carbonate  
 1192 Activated Carbons. Prospect as Sustainable Adsorbent for the Renewable Energy  
 1193 Production. *Journal of Environmental Chemical Engineering*, **2022**, 10 (1),  
 1194 107010. <https://doi.org/10.1016/j.jece.2021.107010>.
- 1195 [55] Marsh, H.; Rodríguez-Reinoso, F. *Activated Carbon*, 1st ed.; Elsevier:  
 1196 Amsterdam ; Boston, 2006.
- 1197 [56] Arami-Niya, A.; Rufford, T. E.; Zhu, Z. Nitrogen-Doped Carbon Foams  
 1198 Synthesized from Banana Peel and Zinc Complex Template for Adsorption of CO  
 1199 <sub>2</sub>, CH<sub>4</sub>, and N<sub>2</sub>. *Energy Fuels*, **2016**, 30 (9), 7298–7309.  
 1200 <https://doi.org/10.1021/acs.energyfuels.6b00971>.
- 1201 [57] Masrurroh, K.; Cahyono, R. B.; Prasetyo, I.; Ariyanto, T. The Effect of Amine  
 1202 Types on Breakthrough Separation of Methane on Biogas. *IJRED*, **2021**, 10 (2),  
 1203 149–155. <https://doi.org/10.14710/ijred.2021.33514>.

- 1204 [58] Prasetyo, I.; Rochmadi, R.; Wahyono, E.; Ariyanto, T. Controlling Synthesis of  
1205 Polymer-Derived Carbon Molecular Sieve and Its Performance for CO<sub>2</sub>/CH<sub>4</sub>  
1206 Separation. *EJ*, **2017**, *21* (4), 83–94. <https://doi.org/10.4186/ej.2017.21.4.83>.
- 1207 [59] Santos, M. P. S.; Grande, C. A.; Rodrigues, A. E. Pressure Swing Adsorption for  
1208 Biogas Upgrading. Effect of Recycling Streams in Pressure Swing Adsorption  
1209 Design. *Ind. Eng. Chem. Res.*, **2011**, *50* (2), 974–985.  
1210 <https://doi.org/10.1021/ie100757u>.
- 1211 [60] Khan, A.; Qyyum, M. A.; Saulat, H.; Ahmad, R.; Peng, X.; Lee, M. Metal–  
1212 Organic Frameworks for Biogas Upgrading: Recent Advancements, Challenges,  
1213 and Future Recommendations. *Applied Materials Today*, **2021**, *22*, 100925.  
1214 <https://doi.org/10.1016/j.apmt.2020.100925>.
- 1215 [61] Liang, Z.; Marshall, M.; Chaffee, A. L. CO<sub>2</sub> Adsorption-Based Separation by  
1216 Metal Organic Framework (Cu-BTC) versus Zeolite (13X). *Energy Fuels*, **2009**,  
1217 *23* (5), 2785–2789. <https://doi.org/10.1021/ef800938e>.
- 1218 [62] Kim, J.; Lee, Y.-R.; Ahn, W.-S. Dry-Gel Conversion Synthesis of Cr-MIL-101  
1219 Aided by Grinding: High Surface Area and High Yield Synthesis with Minimum  
1220 Purification. *Chem. Commun.*, **2013**, *49* (69), 7647.  
1221 <https://doi.org/10.1039/c3cc44559c>.
- 1222 [63] Shen, J.; Wang, X.; Chen, Y. Adsorbents for Adsorption Separation of CO<sub>2</sub> and  
1223 CH<sub>4</sub>: A Literature Review. *Can J Chem Eng*, **2023**, *101* (12), 7115–7133.  
1224 <https://doi.org/10.1002/cjce.24942>.
- 1225 [64] Sharma, H.; Dhir, A. Capture of Carbon Dioxide Using Solid Carbonaceous and  
1226 Non-Carbonaceous Adsorbents: A Review. *Environ Chem Lett*, **2021**, *19* (2), 851–  
1227 873. <https://doi.org/10.1007/s10311-020-01118-2>.
- 1228 [65] Lin, J.-B.; Nguyen, T. T. T.; Vaidhyanathan, R.; Burner, J.; Taylor, J. M.;  
1229 Durekova, H.; Akhtar, F.; Mah, R. K.; Ghaffari-Nik, O.; Marx, S.; et al. A  
1230 Scalable Metal-Organic Framework as a Durable Physisorbent for Carbon Dioxide  
1231 Capture. *Science*, **2021**, *374* (6574), 1464–1469.  
1232 <https://doi.org/10.1126/science.abi7281>.
- 1233 [66] Fujiki, J.; Kajiro, H.; Takakura, Y.; Yajima, T.; Kawajiri, Y. Breakthrough  
1234 Analysis for Parameter Estimation of CO<sub>2</sub> Adsorption on Pelletized Flexible  
1235 Metal–Organic Framework. *Chemical Engineering Journal*, **2023**, *460*, 141781.  
1236 <https://doi.org/10.1016/j.cej.2023.141781>.
- 1237 [67] Salles, F.; Jobic, H.; Ghoufi, A.; Llewellyn, P. L.; Serre, C.; Bourrelly, S.; FØrey,  
1238 Gø.; Maurin, G. Transport Diffusivity of CO<sub>2</sub> in the Highly Flexible Metal–  
1239 Organic Framework MIL-53(Cr)\*. *Angew. Chem.*, **2009**.
- 1240 [68] Ferreira, A. F. P.; Ribeiro, A. M.; Kulaç, S.; Rodrigues, A. E. Methane Purification  
1241 by Adsorptive Processes on MIL-53(Al). *Chemical Engineering Science*, **2015**,  
1242 *124*, 79–95. <https://doi.org/10.1016/j.ces.2014.06.014>.
- 1243 [69] Palomino, M.; Corma, A.; Rey, F.; Valencia, S. New Insights on CO<sub>2</sub>–Methane  
1244 Separation Using LTA Zeolites with Different Si/Al Ratios and a First Comparison  
1245 with MOFs. *Langmuir*, **2010**, *26* (3), 1910–1917.  
1246 <https://doi.org/10.1021/la9026656>.
- 1247 [70] Hou, Y.; Vidu, R.; Stroeve, P. Solar Energy Storage Methods. *Ind. Eng. Chem.*  
1248 *Res.*, **2011**, *50* (15), 8954–8964. <https://doi.org/10.1021/ie2003413>.
- 1249 [71] Wang, Y.; LeVan, M. D. Adsorption Equilibrium of Binary Mixtures of Carbon  
1250 Dioxide and Water Vapor on Zeolites 5A and 13X. *J. Chem. Eng. Data*, **2010**, *55*  
1251 (9), 3189–3195. <https://doi.org/10.1021/je100053g>.
- 1252 [72] Do, D. D. *Adsorption Analysis: Equilibria and Kinetics*; Imperial College Press:  
1253 Queensland, Australia, 1998.



- 1254 [73] Ruthven, D. M. *Principles of Adsorption and Adsorption Processes*, A Wiley-  
1255 Interscience publication.; JOHN WILEY & SONS: United States, 1984.
- 1256 [74] Crittenden, Ba.; Thomas, J. *Adsorption Technology and Design*; Butterworth and  
1257 Heinemann: Great Britain, 1998.
- 1258 [75] Chen, Y.-F.; Lin, P.-W.; Chen, W.-H.; Yen, F.-Y.; Yang, H.-S.; Chou, C.-T.  
1259 Biogas Upgrading by Pressure Swing Adsorption with Design of Experiments.  
1260 *Processes*, **2021**, 9 (8), 1325. <https://doi.org/10.3390/pr9081325>.
- 1261 [76] Saha, D.; Bao, Z.; Jia, F.; Deng, S. Adsorption of CO<sub>2</sub>, CH<sub>4</sub>, N<sub>2</sub>O, and N<sub>2</sub> on  
1262 MOF-5, MOF-177, and Zeolite 5A. *Environ. Sci. Technol.*, **2010**, 44 (5), 1820–  
1263 1826. <https://doi.org/10.1021/es9032309>.
- 1264 [77] Rainone, F.; D'Agostino, O.; Erto, A.; Balsamo, M.; Lancia, A. Biogas Upgrading  
1265 by Adsorption onto Activated Carbon and Carbon Molecular Sieves: Experimental  
1266 and Modelling Study in Binary CO<sub>2</sub>/CH<sub>4</sub> Mixture. *Journal of Environmental*  
1267 *Chemical Engineering*, **2021**, 9 (5), 106256.  
1268 <https://doi.org/10.1016/j.jece.2021.106256>.
- 1269 [78] Li, Y.; Yi, H.; Tang, X.; Li, F.; Yuan, Q. Adsorption Separation of CO<sub>2</sub>/CH<sub>4</sub> Gas  
1270 Mixture on the Commercial Zeolites at Atmospheric Pressure. *Chemical*  
1271 *Engineering Journal*, **2013**, 229, 50–56. <https://doi.org/10.1016/j.cej.2013.05.101>.
- 1272 [79] Arya, A.; Divekar, S.; Rawat, R.; Gupta, P.; Garg, M. O.; Dasgupta, S.; Nanoti, A.;  
1273 Singh, R.; Xiao, P.; Webley, P. A. Upgrading Biogas at Low Pressure by Vacuum  
1274 Swing Adsorption. *Ind. Eng. Chem. Res.*, **2015**, 54 (1), 404–413.  
1275 <https://doi.org/10.1021/ie503243f>.
- 1276 [80] Park, J.-H.; Beum, H.-T.; Kim, J.-N.; Cho, S.-H. Numerical Analysis on the Power  
1277 Consumption of the PSA Process for Recovering CO<sub>2</sub> from Flue Gas. *Ind. Eng.*  
1278 *Chem. Res.*, **2002**, 41 (16), 4122–4131. <https://doi.org/10.1021/ie010716i>.
- 1279 [81] Ruthven, D. M. *Principles of Adsorption and Adsorption Processes*; A Wiley-  
1280 Interscience Publication: United States of America, 1984.
- 1281 [82] Hu, G.; Guo, Y.; Luo, J.; Xiao, G. A Numerical Comparison of Heavy-Purge and  
1282 Dual-Reflux Strategies in Pressure Swing Adsorption for Methane Enrichment.  
1283 *AIChE J.*, **2024**. <https://doi.org/10.1002/aic.18573>.
- 1284 [83] Kim, J.-N.; Chue, K.-T.; Cho, S.-H.; Kim, J.-D. Production of High-Purity  
1285 Nitrogen from Air by Pressure Swing Adsorption on Zeolite X. *Separation Science*  
1286 *and Technology*, **1995**, 30 (3), 347–368.  
1287 <https://doi.org/10.1080/01496399508013876>.
- 1288 [84] Li, H.; Liao, Z.; Sun, J.; Jiang, B.; Wang, J.; Yang, Y. Modelling and Simulation  
1289 of Two-Bed PSA Process for Separating H<sub>2</sub> from Methane Steam Reforming.  
1290 *Chinese Journal of Chemical Engineering*, **2019**, 27 (8), 1870–1878.  
1291 <https://doi.org/10.1016/j.cjche.2018.11.022>.
- 1292 [85] Paz, L.; Grekov, D. I.; Pré, P. Dynamics of Hydrogen Storage through Adsorption:  
1293 Process Simulation and Energy Analysis. *Processes*, **2023**, 11 (10), 2940.  
1294 <https://doi.org/10.3390/pr11102940>.
- 1295 [86] Delgado, J. A.; Uguina, M. A.; Sotelo, J. L.; Ruíz, B.; Gómez, J. M. Fixed-Bed  
1296 Adsorption of Carbon Dioxide/Methane Mixtures on Silicalite Pellets. *Adsorption*,  
1297 **2006**, 12 (1), 5–18. <https://doi.org/10.1007/s10450-006-0134-3>.
- 1298 [87] Thomas, W. J.; Crittenden, B. D. *Adsorption Technology and Design*;  
1299 Butterworth-Heinemann: Oxford ; Boston, 1998.
- 1300 [88] Khalighi, M.; Farooq, S.; Karimi, I. A. Nonisothermal Pore Diffusion Model for a  
1301 Kinetically Controlled Pressure Swing Adsorption Process. *Ind. Eng. Chem. Res.*,  
1302 **2012**, 51 (32), 10659–10670. <https://doi.org/10.1021/ie3004539>.

- 1303 [89] Fakhroleslam, M.; Fatemi, S. Comparative Simulation Study of PSA, VSA, and  
1304 TSA Processes for Purification of Methane from CO<sub>2</sub> via SAPO-34 Core-Shell  
1305 Adsorbent. *Separation Science and Technology*, **2016**, *51* (14), 2326–2338.  
1306 <https://doi.org/10.1080/01496395.2016.1210640>.
- 1307 [90] Ali Abd, A.; Roslee Othman, M. Biogas Upgrading to Fuel Grade Methane Using  
1308 Pressure Swing Adsorption: Parametric Sensitivity Analysis on an Industrial Scale.  
1309 *Fuel*, **2022**, *308*, 121986. <https://doi.org/10.1016/j.fuel.2021.121986>.
- 1310 [91] Abd, A. A.; Othman, M. R.; Shamsudin, I. K.; Helwani, Z.; Idris, I. Biogas  
1311 Upgrading to Natural Gas Pipeline Quality Using Pressure Swing Adsorption for  
1312 CO<sub>2</sub> Separation over UiO-66: Experimental and Dynamic Modelling Assessment.  
1313 *Chemical Engineering Journal*, **2023**, *453*, 139774.  
1314 <https://doi.org/10.1016/j.cej.2022.139774>.
- 1315 [92] De Witte, N.; Denayer, J. F. M.; Van Assche, T. R. C. Effect of Adsorption  
1316 Duration and Purge Flowrate on Pressure Swing Adsorption Performance. *Ind.*  
1317 *Eng. Chem. Res.*, **2021**, *60* (37), 13684–13691.  
1318 <https://doi.org/10.1021/acs.iecr.1c02291>.
- 1319 [93] Chouikhi, N.; Brandani, F.; Pullumbi, P.; Perre, P.; Puel, F. Biomethane  
1320 Production by Adsorption Technology: New Cycle Development, Adsorbent  
1321 Selection and Process Optimization. *Adsorption*, **2020**, *26* (8), 1275–1289.  
1322 <https://doi.org/10.1007/s10450-020-00250-3>.
- 1323 [94] Grande, C. A.; Rodrigues, A. E. Propane/Propylene Separation by Pressure Swing  
1324 Adsorption Using Zeolite 4A. *Ind. Eng. Chem. Res.*, **2005**, *44* (23), 8815–8829.  
1325 <https://doi.org/10.1021/ie050671b>.
- 1326 [95] Grande, C. A.; Blom, R.; Möller, A.; Möllmer, J. High-Pressure Separation of  
1327 CH<sub>4</sub>/CO<sub>2</sub> Using Activated Carbon. *Chemical Engineering Science*, **2013**, *89*, 10–  
1328 20. <https://doi.org/10.1016/j.ces.2012.11.024>.
- 1329 [96] Santos, M. S.; Grande, C. A.; Rodrigues, A. E. New Cycle Configuration to  
1330 Enhance Performance of Kinetic PSA Processes. *Chemical Engineering Science*,  
1331 **2011**, *66* (8), 1590–1599. <https://doi.org/10.1016/j.ces.2010.12.032>.
- 1332 [97] Cavenati, S.; Grande, C. A.; Rodrigues, A. E. Separation of CH<sub>4</sub> / CO<sub>2</sub> / N<sub>2</sub>  
1333 Mixtures by Layered Pressure Swing Adsorption for Upgrade of Natural Gas.  
1334 *Chemical Engineering Science*, **2006**, *61* (12), 3893–3906.  
1335 <https://doi.org/10.1016/j.ces.2006.01.023>.
- 1336 [98] Lemmon, E. W.; Huber, M. L.; McLinden, M. O. NIST Standard Reference  
1337 Database 23: Reference Fluid Thermodynamic and Transport Properties-  
1338 REFPROP, 2018.
- 1339 [99] Biegler, L. T.; Jiang, L.; Fox, V. G. Recent Advances in Simulation and Optimal  
1340 Design of Pressure Swing Adsorption Systems. *Separation & Purification*  
1341 *Reviews*, **2005**, *33* (1), 1–39. <https://doi.org/10.1081/SPM-120039562>.
- 1342 [100] Liu, Y.; Delgado, J.; Ritter, J. A. Comparison of Finite Difference Techniques  
1343 for Simulating Pressure Swing Adsorption. **1998**.
- 1344 [101] Young, L. C. Orthogonal Collocation Revisited. *Computer Methods in Applied*  
1345 *Mechanics and Engineering*, **2019**, *345*, 1033–1076.  
1346 <https://doi.org/10.1016/j.cma.2018.10.019>.
- 1347 [102] Khajuria, H.; Pistikopoulos, E. N. Dynamic Modeling and Explicit/Multi-  
1348 Parametric MPC Control of Pressure Swing Adsorption Systems. *Journal of*  
1349 *Process Control*, **2011**, *21* (1), 151–163.  
1350 <https://doi.org/10.1016/j.jprocont.2010.10.021>.

- 1351 [103] Zhang, R.; Shen, Y.; Tang, Z.; Li, W.; Zhang, D. A Review of Numerical  
1352 Research on the Pressure Swing Adsorption Process. *Processes*, **2022**, *10* (5), 812.  
1353 <https://doi.org/10.3390/pr10050812>.
- 1354 [104] Kadam, R. S.; Yadav, G. D. Pressure Swing Distillation: Heat Integration and  
1355 Economics. *Separation & Purification Reviews*, **2024**, 1–27.  
1356 <https://doi.org/10.1080/15422119.2024.2306595>.
- 1357 [105] Kim S.; Ko D.; Moon I. Dynamic Optimization of CH<sub>4</sub>/CO<sub>2</sub> Separating  
1358 Operation Using Pressure Swing Adsorption Process with Feed Composition  
1359 Varies. *Chemical Engineering Transactions*, **2015**, *45*, 853–858.  
1360 <https://doi.org/10.3303/CET1545143>.
- 1361 [106] Kapoor, A.; Yang, R. T. Kinetic Separation of Methane—Carbon Dioxide  
1362 Mixture by Adsorption on Molecular Sieve Carbon. *Chemical Engineering  
1363 Science*, **1989**, *44* (8), 1723–1733. [https://doi.org/10.1016/0009-2509\(89\)80014-4](https://doi.org/10.1016/0009-2509(89)80014-4).
- 1364 [107] Cavenati, S.; Grande, C. A.; Rodrigues, A. E. Upgrade of Methane from Landfill  
1365 Gas by Pressure Swing Adsorption. *Energy Fuels*, **2005**, *19* (6), 2545–2555.  
1366 <https://doi.org/10.1021/ef050072h>.
- 1367 [108] Durán, I.; Rubiera, F.; Pevida, C. Modeling a Biogas Upgrading PSA Unit with  
1368 a Sustainable Activated Carbon Derived from Pine Sawdust. Sensitivity Analysis  
1369 on the Adsorption of CO<sub>2</sub> and CH<sub>4</sub> Mixtures. *Chemical Engineering Journal*,  
1370 **2022**, *428*, 132564. <https://doi.org/10.1016/j.cej.2021.132564>.
- 1371 [109] Grande, C. A.; Rodrigues, A. E. Biogas to Fuel by Vacuum Pressure Swing  
1372 Adsorption I. Behavior of Equilibrium and Kinetic-Based Adsorbents. *Ind. Eng.  
1373 Chem. Res.*, **2007**, *46* (13), 4595–4605. <https://doi.org/10.1021/ie061341+>.
- 1374 [110] Berlin, N. H. Vacuum Cycle Adsorption. 3,313,091, April 11, 1967.
- 1375 [111] Kim, M.-B.; Bae, Y.-S.; Choi, D.-K.; Lee, C.-H. Kinetic Separation of Landfill  
1376 Gas by a Two-Bed Pressure Swing Adsorption Process Packed with Carbon  
1377 Molecular Sieve: Nonisothermal Operation. *Ind. Eng. Chem. Res.*, **2006**, *45* (14),  
1378 5050–5058. <https://doi.org/10.1021/ie0511074>.
- 1379 [112] Canevesi, R. L. S.; Andreassen, K. A.; Silva, E. A.; Borba, C. E.; Grande, C. A.  
1380 Evaluation of Simplified Pressure Swing Adsorption Cycles for Bio-Methane  
1381 Production. *Adsorption*, **2019**, *25* (4), 783–793. <https://doi.org/10.1007/s10450-019-00049-x>.
- 1383 [113] Shen, Y.; Shi, W.; Zhang, D.; Na, P.; Fu, B. The Removal and Capture of CO<sub>2</sub>  
1384 from Biogas by Vacuum Pressure Swing Process Using Silica Gel. *Journal of CO<sub>2</sub>  
1385 Utilization*, **2018**, *27*, 259–271. <https://doi.org/10.1016/j.jcou.2018.08.001>.
- 1386 [114] Vilardi, G.; Bassano, C.; Deiana, P.; Verdone, N. Exergy and Energy Analysis  
1387 of Biogas Upgrading by Pressure Swing Adsorption: Dynamic Analysis of the  
1388 Process. *Energy Conversion and Management*, **2020**, *226*, 113482.  
1389 <https://doi.org/10.1016/j.enconman.2020.113482>.
- 1390 [115] Augelletti, R.; Conti, M.; Annesini, M. C. Pressure Swing Adsorption for Biogas  
1391 Upgrading. A New Process Configuration for the Separation of Biomethane and  
1392 Carbon Dioxide. *Journal of Cleaner Production*, **2017**, *140*, 1390–1398.  
1393 <https://doi.org/10.1016/j.jclepro.2016.10.013>.
- 1394 [116] Moseley, P. T.; Rand, D. A. J.; Davidson, A.; Monahov, B. Understanding the  
1395 Functions of Carbon in the Negative Active-Mass of the Lead–Acid Battery: A  
1396 Review of Progress. *Journal of Energy Storage*, **2018**, *19*, 272–290.  
1397 <https://doi.org/10.1016/j.est.2018.08.003>.
- 1398 [117] Cosey, W. K.; Balkus, K. J.; Ferraris, J. P.; Musselman, I. H. Reduced Aging in  
1399 Carbon Molecular Sieve Membranes Derived from PIM-1 and MOP-18. *Ind. Eng.  
1400 Chem. Res.*, **2021**, *60* (27), 9962–9970. <https://doi.org/10.1021/acs.iecr.1c01727>.

- 1401 [118] León, M.; Silva, J.; Carrasco, S.; Barrientos, N. Design, Cost Estimation and  
 1402 Sensitivity Analysis for a Production Process of Activated Carbon from Waste  
 1403 Nutshells by Physical Activation. *Processes*, **2020**, *8* (8), 945.  
 1404 <https://doi.org/10.3390/pr8080945>.
- 1405 [119] Peng, P.; Anastasopoulou, A.; Brooks, K.; Furukawa, H.; Bowden, M. E.; Long,  
 1406 J. R.; Autrey, T.; Breunig, H. Cost and Potential of Metal–Organic Frameworks  
 1407 for Hydrogen Back-up Power Supply. *Nat Energy*, **2022**, *7* (5), 448–458.  
 1408 <https://doi.org/10.1038/s41560-022-01013-w>.
- 1409 [120] DeSantis, D.; Mason, J. A.; James, B. D.; Houchins, C.; Long, J. R. Techno-  
 1410 Economic Analysis of Metal-Organic Frameworks for Hydro- Gen and Natural  
 1411 Gas Storage. *Energy & Fuels*, **2017**, *31*, 2024–2032.  
 1412 <https://doi.org/10.1021/acs.energyfuels.6b02510>.
- 1413 [121] Abdalla, Nabil; Bürck, Silvana; Fehrenbach, Horst; Köpen, Susanne; Staigl, Tim  
 1414 Janosch. *Biomethane in Europe*; Prepared on behalf of the European Climate  
 1415 Foundation; ifeu: Heidelberg, 2022.
- 1416 [122] Alberici, Sacha; Grimme, Wouter; Toop, Gemma. *Biomethane Production*  
 1417 *Potentials in the EU - Feasibility of REPowerEU 2030 Targets, Production*  
 1418 *Potentials in the Member States and Outlook to 2050*; A gas for climate report;  
 1419 Guidehouse, 2022.
- 1420 [123] Álvarez-Gutiérrez, N. Towards Bio-Upgrading of Biogas: Biomass Waste-Based  
 1421 Adsorbents. *Energy Procedia*, **2014**, No. 63, 6527–6533.  
 1422 <https://doi.org/10.1016/j.egypro.2014.11.688>.
- 1423 [124] Gil, M. V.; Álvarez-Gutiérrez, N.; Martínez, M.; Rubiera, F.; Pevida, C.; Morán,  
 1424 A. Carbon Adsorbents for CO<sub>2</sub> Capture from Bio-Hydrogen and Biogas Streams:  
 1425 Breakthrough Adsorption Study. *Chemical Engineering Journal*, **2015**, *269*, 148–  
 1426 158. <https://doi.org/10.1016/j.cej.2015.01.100>.
- 1427 [125] Liu, F.; Zhang, Y.; Zhang, P.; Xu, M.; Tan, T.; Wang, J.; Deng, Q.; Zhang, L.;  
 1428 Wan, Y.; Deng, S. Facile Preparation of N and O-Rich Porous Carbon from Palm  
 1429 Sheath for Highly Selective Separation of CO<sub>2</sub>/CH<sub>4</sub>/N<sub>2</sub> Gas-Mixture. *Chemical*  
 1430 *Engineering Journal*, **2020**, *399*, 125812.  
 1431 <https://doi.org/10.1016/j.cej.2020.125812>.
- 1432 [126] Prasetyo, I.; Mukti, N. I. F.; Cahyono, R. B.; Prasetya, A.; Ariyanto, T.  
 1433 Nanoporous Carbon Prepared from Palm Kernel Shell for CO<sub>2</sub>/CH<sub>4</sub> Separation.  
 1434 *Waste Biomass Valor*, **2020**, *11* (10), 5599–5606. [https://doi.org/10.1007/s12649-](https://doi.org/10.1007/s12649-020-01006-4)  
 1435 [020-01006-4](https://doi.org/10.1007/s12649-020-01006-4).
- 1436 [127] Rocha, L. A. M.; Andreassen, K. A.; Grande, C. A. Separation of CO<sub>2</sub>/CH<sub>4</sub>  
 1437 Using Carbon Molecular Sieve (CMS) at Low and High Pressure. *Chemical*  
 1438 *Engineering Science*, **2017**, *164*, 148–157.  
 1439 <https://doi.org/10.1016/j.ces.2017.01.071>.
- 1440 [128] Kim, Y. J.; Nam, Y. S.; Kang, Y. T. Study on a Numerical Model and PSA  
 1441 (Pressure Swing Adsorption) Process Experiment for CH<sub>4</sub>/CO<sub>2</sub> Separation from  
 1442 Biogas. *Energy*, **2015**, *91*, 732–741. <https://doi.org/10.1016/j.energy.2015.08.086>.
- 1443 [129] Cavenati, S.; Grande, C. A.; Rodrigues, A. E.; Kiener, C.; Müller, U. Metal  
 1444 Organic Framework Adsorbent for Biogas Upgrading. *Ind. Eng. Chem. Res.*, **2008**,  
 1445 *47* (16), 6333–6335. <https://doi.org/10.1021/ie8005269>.
- 1446 [130] Hamon, L.; Heymans, N.; Llewellyn, P. L.; Guillerm, V.; Ghoufi, A.; Vaesen,  
 1447 S.; Maurin, G.; Serre, C.; De Weireld, G.; Pirngruber, G. D. Separation of CO<sub>2</sub>–  
 1448 CH<sub>4</sub> Mixtures in the Mesoporous MIL-100(Cr) MOF: Experimental and  
 1449 Modelling Approaches. *Dalton Trans.*, **2012**, *41* (14), 4052.  
 1450 <https://doi.org/10.1039/c2dt12102f>.

- 1451 [131] Chen, R.; Yao, J.; Gu, Q.; Smeets, S.; Baerlocher, C.; Gu, H.; Zhu, D.; Morris,  
1452 W.; Yaghi, O. M.; Wang, H. A Two-Dimensional Zeolitic Imidazolate Framework  
1453 with a Cushion-Shaped Cavity for CO<sub>2</sub> Adsorption. *Chem. Commun.*, **2013**, 49  
1454 (82), 9500. <https://doi.org/10.1039/c3cc44342f>.
- 1455 [132] Abid, H. R.; Pham, G. H.; Ang, H.-M.; Tade, M. O.; Wang, S. Adsorption of  
1456 CH<sub>4</sub> and CO<sub>2</sub> on Zr-Metal Organic Frameworks. *Journal of Colloid and Interface*  
1457 *Science*, **2012**, 366 (1), 120–124. <https://doi.org/10.1016/j.jcis.2011.09.060>.
- 1458
- 1459


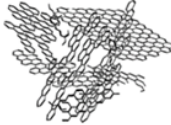
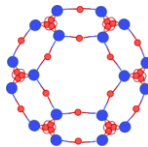
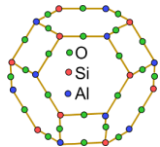
1460 **Table 1.** Typical biogas composition (%).<sup>[1]</sup>

Components	Agricultural waste	Landfill gas	Industrial waste
Methane, CH <sub>4</sub>	50 - 80	50 - 80	50 - 70
Carbon dioxide, CO <sub>2</sub>	30 - 50	20 - 50	30 - 50
Hydrogen sulfide, H <sub>2</sub> S	0.70	0.10	0.80
Hydrogen, H <sub>2</sub>	0 - 2	0 - 5	0 - 2
Nitrogen, N <sub>2</sub>	0 - 1	0 - 3	0 - 1
Oxygen, O <sub>2</sub>	0 - 1	0 - 1	0 - 1
Carbon monoxide, CO	0 - 1	0 - 1	0 - 1
Ammonia, NH <sub>3</sub>	Traces	Traces	Traces
Siloxanes	Traces	Traces	Traces
Water, H <sub>2</sub> O	Saturation	Saturation	Saturation

1461

1462





1463 **Table 2.** Comparison of the properties of activated carbons, carbon molecular sieves,  
 1464 metal organic frameworks and zeolites. AC and CMS images were taken with  
 1465 permission from <sup>[116]</sup> and <sup>[117]</sup>.

	Activated carbon	Carbon molecular sieve	Metal organic framework	Zeolite
				
<b>Nature</b>	Carbonaceous	Carbonaceous	Organic ligands and metal ions	Crystalline aluminosilicates
<b>Pore size distribution (PSD)</b>	Wide PSD: micropores (<2 nm) and mesopores (2-50 nm)	Narrow PSD (<1 nm)	Tailorable PSD	Uniform and narrow PSD (<1 nm)
<b>Adsorption mechanism</b>	Presence of micropores and active sites	Well-defined micropores	Well-defined micropores	Well-defined micropores
<b>Surface area</b>	High due to micropores and mesopores	High due to micropores	High due to micropores	High due to micropores

1466

1467

1468 **Table 3.** Main properties of adsorbents for CO<sub>2</sub>/CH<sub>4</sub> separation.

	Activated carbon	Carbon molecular sieve	Metal organic framework	Zeolite
				
<b>CO<sub>2</sub> adsorption capacity</b>	High	Medium	Medium	High
<b>CH<sub>4</sub> adsorption capacity</b>	High	Medium	Low	Low
<b>CO<sub>2</sub>/CH<sub>4</sub> equilibrium selectivity</b>	Low	Low	Medium	High
<b>CO<sub>2</sub>/CH<sub>4</sub> kinetic selectivity</b>	Low	High	Medium	High
<b>PSA regeneration</b>	Feasible	Feasible	Not documented	Feasible at P < P <sub>tam</sub>
<b>Cost (USD kg<sup>-1</sup>)</b>	0.6 – 2.4 <sup>[118]</sup>	6.0 – 15.0	10.0 – 70.0 <sup>[119, 120]</sup>	0.6 – 5.0

1469

1470

1471 **Table 4.** Summary of dynamic models for CO<sub>2</sub>/CH<sub>4</sub> separation through PSA systems.

System-Adsorbent	Cycle steps	Flow pattern	Isotherm	Mass transfer kinetics	Gas behaviour	Heat effects	Solver	Ref.
2bed - Silicalite	1. Feed/PR - 2. ADS -3. BD - 4.PG	ADPF	MLM	LDF	Ideal	LTE	PDECOL software using orthogonal collocation on finite elements	[86]
2bed - Zeolite 13X	1. Feed/PR - 2. ADS - 3. DPE - 4. BD - 5. PG - 6. PPE	ADPF	MLM	bi-LDF	Ideal	No LTE	gPROMS software using centered finite difference of second order over a grid of 250 intervals	[59]
4bed - MOF MIL 53	1. Product/PR - 2. ADS - 3. Rinse - 4. BD - 5. PG	ADPF	MLM	LDF	Ideal	No LTE	gPROMS software using orthogonal collocation on finite elements with second order polynomials and 50 intervals	[68]
2bed - Zeolite SAPO 34	1. Feed/PR - 2. ADS - 3. DPE - 4. BD - 5. PG - 6. PPE	ADPF	MLM	LDF	Ideal	LTE	Orthogonal collocation and method of lines	[89]
1bed - Zeolite and CMS	1. Feed/PR - 2. ADS -3. BD - 4.PG	-	MLM	LDF	-	No LTE	Aspen Adsorption TM version 10	[90]
1bed - Activated carbon	-	ADPF	MLM	bi-LDF	BWR correlation	LTE	gPROMS software using centered finite difference of second order over a grid of 400 intervals	[95]
4bed - Zeolite 13X and CMS 3K	1. Product/PR - 2. Product and production - 3. ADS - 4. ADS - 5. ADS - 6. DPE - 7. BD - 8. PG - 9. PPE	ADPF	MLM	bi-LDF	Ideal	No LTE	gPROMS software using centered finite difference over a grid of 200 intervals	[96]
1bed - Zeolite 13X + CMS 3K	1. Feed/PR - 2. ADS -3. BD - 4.PG	ADPF	MLM	bi-LDF	-	No LTE	gPROMS software using orthogonal collocation on finite elements	[97]
2bed - UiO66 MOF	1. Feed/PR - 2. ADS -3. BD - 4.PG	ADPF	MLM	LDF	Ideal	No LTE	Aspen Adsorption using as finite difference method, the upwind	[91]



2bed – FAU Zeolite 13X	1. Feed/PR – 2. ADS – 3. DPE – 4. BD – 5. PG – 6. PPE	ADPF	MLM	LDF	Peng-Robinson equation	No LTE	Aspen Adsorption V9	[92]
5bed - CMS	1. Feed/PR – 2. ADS – 3. ADS/reflux – 4. DPE – 5. PG – 6. DPE – 7. BD – 8. BD/Reflux – 9. PPE – 10. Idle – 11. PPE	ADPF	MLM	bi-LDF	Ideal	No LTE	FORTRAN using the finite difference method	[93]

1472

1473 **Table 5.** Single-bed PSA technologies for CO<sub>2</sub>/CH<sub>4</sub> separation.

Cycle - time (s)	Cycle steps	Adsorbent	CO <sub>2</sub> /CH <sub>4</sub>	P <sub>a</sub> – P <sub>d</sub> (atm)	CH <sub>4</sub> Purity (%) - CH <sub>4</sub> Recovery (%)	Productivity (mol <sub>CH4</sub> kg <sup>-1</sup> h <sup>-1</sup> ) - Energy consumption (KWh mol <sub>CH4</sub> <sup>-1</sup> )	Ref.
VSA - 120	1. Feed/PR - 2. ADS - 3. BD - 4. PG	CMS Bergbau Forschung	50/50	3.7 - 0.3	95.0 - 58.0	1.7 <sup>a</sup> - 0.0050 <sup>a</sup>	[106]
		Zeolite 5A		2.0 - 0.3	75.9 - 86.4	0.8 <sup>a</sup> - 0.0031 <sup>a</sup>	
VSA - 370	1. Feed/PR - 2. ADS - 3. BD - 4. PG	CMS 3K	45/55	3.2 - 0.1	97.1 - 79.4	3.2 <sup>a</sup> - 0.0068 <sup>a</sup>	[107]
VSA - 425	1. Product/PR - 2. ADS - 3. Intermediate DP - 4. BD - 5. PG	CMS 3K	55/45	7.9 - 0.1	97.3 - 85.6	4.3 - 0.0153 <sup>a</sup>	[109]
VSA - 470	1. Feed/PR - 2. ADS - 3. Intermediate DP - 4. BD - 5. PG	Zeolite 13X			97.1 - 60.7	4.4 - 0.0190 <sup>a</sup>	
PSA - 1200	1. Feed/PR - 2. ADS - 3. BD - 4. PG	MIL-53	40/60	4.0 - 1.0	94.4 - 35.5	2.5 - 0.0128 <sup>a</sup>	[68]
PSA - 1680	1. Feed/PR - 2. ADS - 3. BD, He regeneration - 4. PG	Sawdust Activated Carbon	50/50	4.0 - 1.0	97.0 - 60.0	2.8 <sup>a</sup> - 0.0047 <sup>a</sup>	[108]

1474 <sup>a</sup> Calculated in this work

1475

1476

**Table 6.** Multi-bed PSA technologies for CO<sub>2</sub>/CH<sub>4</sub> separation - experimental studies.

Cycle - time (s)	Cycle steps	Adsorbent	CO <sub>2</sub> /CH <sub>4</sub>	P <sub>a</sub> - P <sub>d</sub> (atm)	CH <sub>4</sub> Purity (%) - CH <sub>4</sub> Recovery (%)	Productivity (mol <sub>CH<sub>4</sub></sub> kg <sup>-1</sup> h <sup>-1</sup> ) - Energy consumption (KWh mol <sub>CH<sub>4</sub></sub> <sup>-1</sup> )	Ref.
2bed EPSA - 480	1. Feed/PR - 2. ADS - 3. DPE - 4. BD - 5. PG - 6. PPE	CMS Takeda 3A	50/50	4.0 - 1.0	95.8 - 71.2	5.8 - 0.0056 <sup>a</sup>	[111]
2bed EVSA - 362		13X Zeolite Z10-04			90.2 - 92.7	14.1 - 0.0033 <sup>a</sup>	
2bed EVSA - 182	1.Feed/PR -2. ADS - 3. DPE - 4. BD - 5. PPE.	Zeolite KZ10-04	42/58	1.5 - 0.1	91.2 - 83.7	11.9 - 0.0039 <sup>a</sup>	[79]
2bed EVSA - 336		Zeolite NaUSY			99.3 - 85.9	15.6 - 0.0039 <sup>a</sup>	
2bed EVSA - 290		CMS 3K			96.9 - 86.9	11.3 - 0.0038 <sup>a</sup>	
2bed VSA - 140	1. Feed/PR - 2. ADS - 3. DPE - 4. BD - 5. PPE	Zeolite NaUSY	50/50	2.0 - 0.1	99.0 - 73.0	12.8 <sup>a</sup> - 0.0044 <sup>a</sup>	[39]
4bed EVSA - 600	1. Feed/PR - 2. ADS - 3. DPE1 - 4. IDLE - 5. DPE2 - 6. BD - 7. PG - 8. PPE1 - 9. PPE2	Silica gel	45/55	4.0 - 0.3	98.3 - 73.1	2.9 <sup>a</sup> - 0.0036	[113]
2bed-1tank EVSA - 1800	1. Feed/PR - 2. ADS - 3. DPE - 4. BD - 5. PG - 6. PPE				97.9 - 91.0	3.8 - 0.0085 <sup>a</sup>	
3bed-1tank EVSA - 1560	1. Feed/PR - 2. ADS - 3. Idle - 4. DPE1 and DPE2 - 5. BD - 6. PPE1 and PPE2.	CMS KP 407	40/60	1.5 - 0.1	98.4 - 92.1	2.6 - 0.0084 <sup>a</sup>	[112]
2bed EVSA - 336	1. Feed/PR - 2. AD - 3. DPE - 4. DP - 5. BD - 6. PPE	COSMO Zeolite 13X	36/64	4.0 - 0.1	95.5 - 91.3	3.3 <sup>a</sup> - 0.0072 <sup>a</sup>	[75]

**Table 7.** Multi-bed PSA technologies for CO<sub>2</sub>/CH<sub>4</sub> separation - simulation studies.

Cycle - time (s)	Cycle steps	Adsorbent	CO <sub>2</sub> /CH <sub>4</sub>	P <sub>A</sub> - P <sub>D</sub> (atm)	CH <sub>4</sub> Purity (%) - CH <sub>4</sub> Recovery (%)	Productivity (mol <sub>CH<sub>4</sub></sub> kg <sup>-1</sup> h <sup>-1</sup> ) - Energy consumption (KWh mol <sub>CH<sub>4</sub></sub> <sup>-1</sup> )	Ref.
2bed VSA - 80	1. Feed/PR - 2. ADS - 3. BD - 4. PG	Silicalite	38/62	1.0 - 0.1	97.8 - 58.5	8.6 -	[86]
2bed VSA - 400	1. Feed/PR - 2. ADS - 3. Intermediate depressurization - 4. BD - 5. PG	2 layers: CMS-3K and Zeolite 13X	45/55	7.9 - 0.1	98.0 - 80.3	7.7 - 0.0069 <sup>a</sup>	[38]
2bed EVSA - 850	1. Feed/PR - 2. ADS - 3. DPE - 4. BD - 5. PG - 6. PPE	Zeolite 13X	33/67	4.0 - 0.3	99.2 - 85.0	5.9 - 0.0086 <sup>a</sup>	[59]
4bed VSAm <sup>c</sup> - 1080 <sup>b</sup>	1. Product/PR - 2. ADS - 3. Rinse - 4. BD - 5. PG	MIL-53	40/60	4.0 - 0.1	99.4 - 92.8	2.1 - 0.0170	[68]
2bed EVSA - 850 <sup>b</sup>	1. Feed/PR - 2. AD - 3. DPE - 4. BD - 5. PG - 6. PPE	COSMO Zeolite 13X	36/64	4.5 - 0.1	97.0 - 95.4	12.8 <sup>a</sup> - 0.0076 <sup>a</sup>	[75]
2bed PSA -	1. Feed/PR - 2. ADS - 3. BD - 4. PG	Spent coffee	32/68	2.0 - 1.0	97.0 - 95.4	-	[2]
4bed EVSA - 520 (2 systems) <sup>b</sup>	1. Feed/PR - 2. ADS - 3. DPE - 4. BD - 5. PG - 6. PPE (each system)	Zeolite 5A	37/63	6.2-0.2	99.4 - 99.0	8.2 <sup>a</sup> - 0.0056	[115]
6bed VSA - 240	1. Feed/PR - 2. ADS - 3. BD - 4. PG	CMS-3K	45/55	6.5-0.3	97.1 - 93.4	8.9 - 0.0058	[114]
5bed EVSA - 725 <sup>b</sup>	1. Feed/PR - 2. ADS - 3. ADS/reflux - 4. DPE - 5. PG - 6. DPE - 7. BD - 8. BD/Reflux - 9. PPE - 10. Idle - 11. PPE	CMS	40/60	8.0 - 0.5	97.0 - 87.3	1.2 - 0.0093	[93]

1480

<sup>a</sup> Calculated by this work

1481

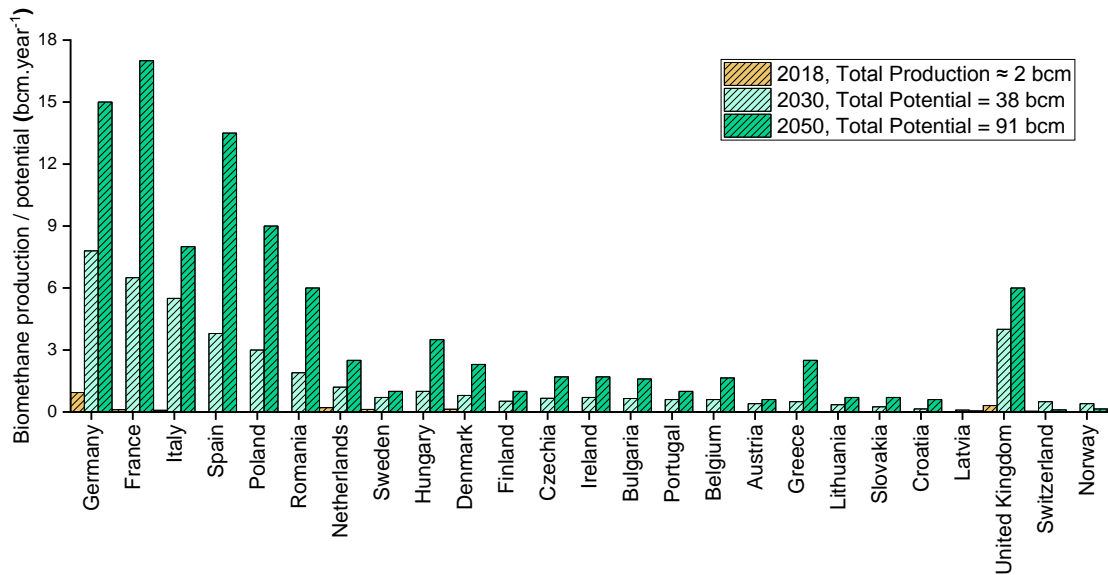
<sup>b</sup> Industrial scale-up

1482

<sup>c</sup> VSAm: VSA cycle modified.

1483

1484



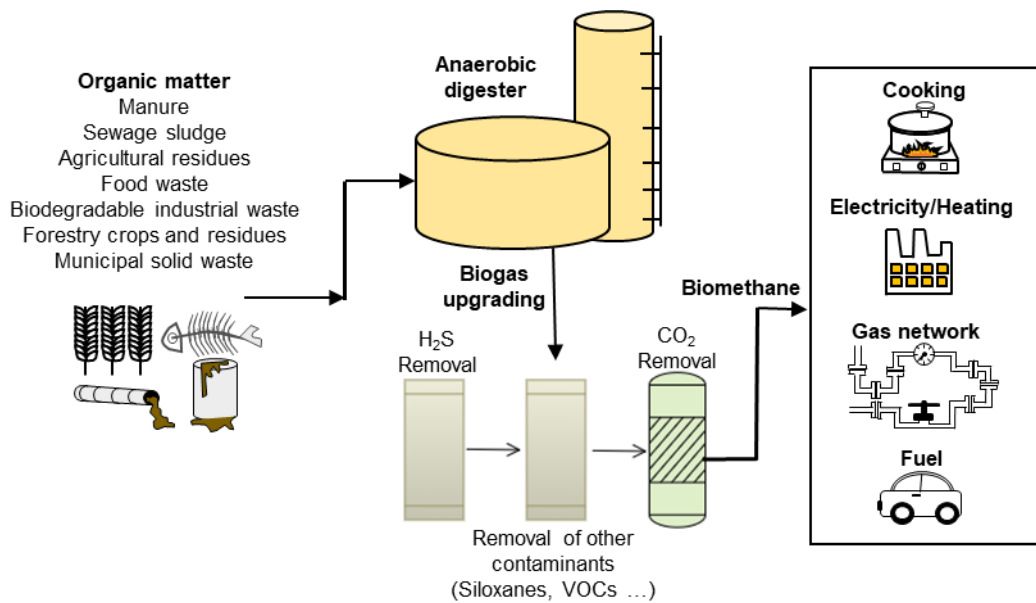
1485

1486 **Figure 1.** Current<sup>[121]</sup> and potential production in 2030 and 2050<sup>[122]</sup> of biomethane per  
 1487 country from anaerobic digestion in Europe, expressed in billion cubic meters (bcm).

1488 NB: the natural gas consumption in the UE in 2020 was 400 bcm.<sup>[122]</sup>

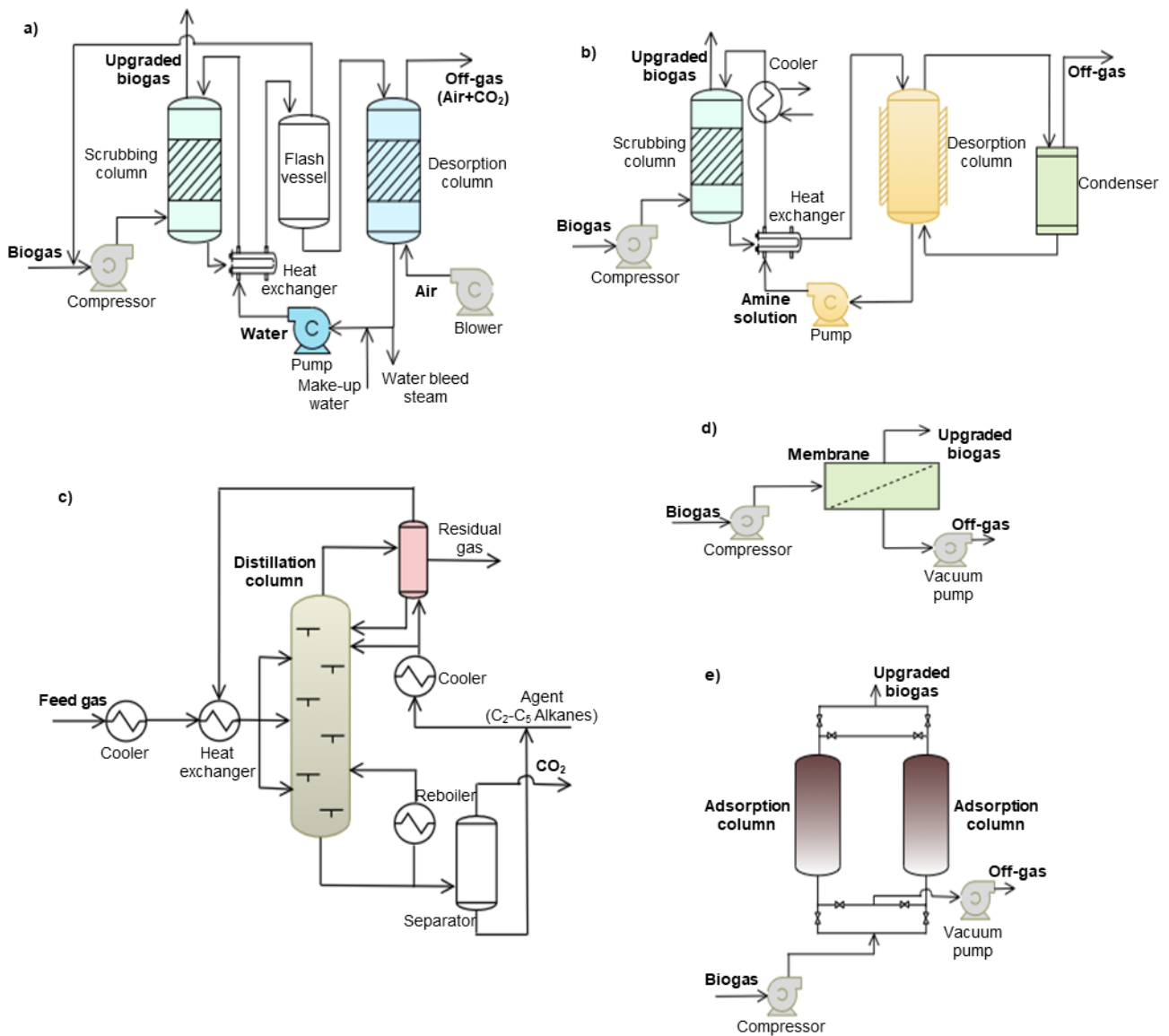
1489

1490

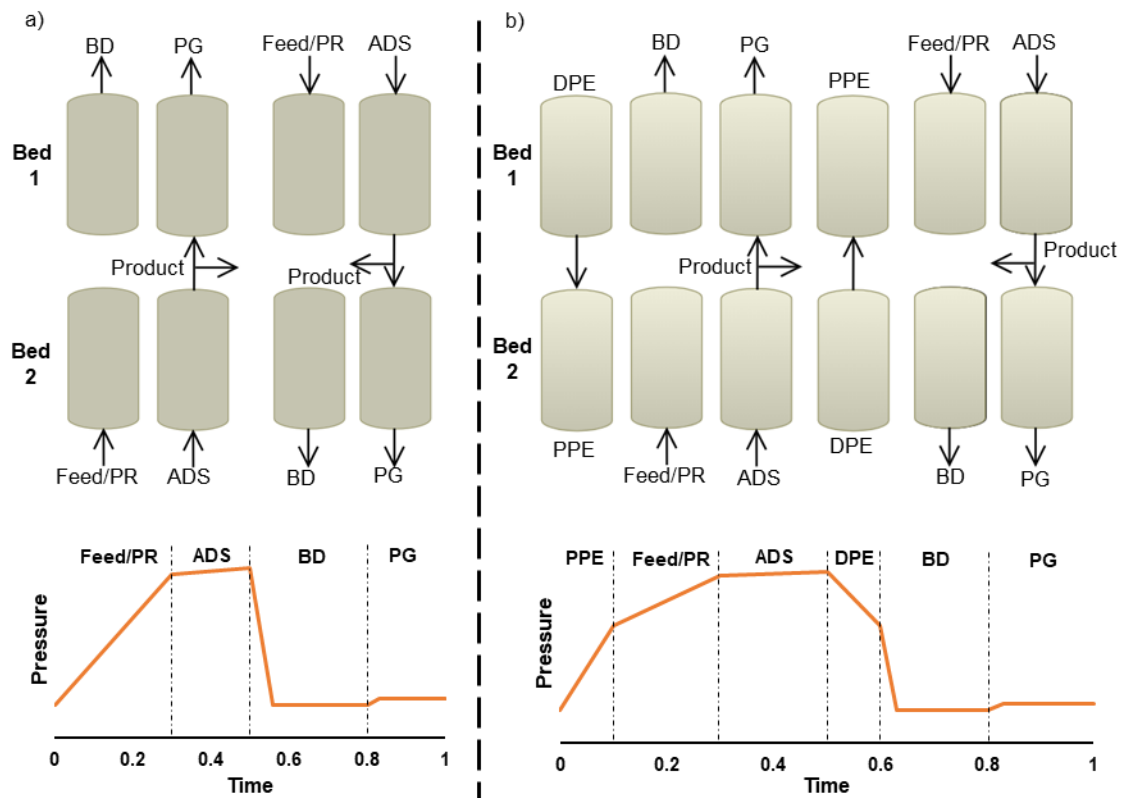


1491

1492 **Figure 2.** Biomethane production and its applications.



1493 **Figure 3.** Schematic diagrams of biogas upgrading methods: a) water scrubbing; b)  
 1494 chemical scrubbing (amine scrubbing); c) cryogenic distillation; d) membrane  
 1495 separation; e) pressure swing adsorption.



1496

1497 **Figure 4.** Sequence steps for: a) basic Skarstrom PSA cycle; and b) EPSA cycle.

1498 *Product/PR*: pressurization with product; *ADS*: adsorption; *BD*: blowdown; *PG*: purge;

1499 *Intermediate DP*: intermediate depressurization; *DPE*: Depressurization pressure

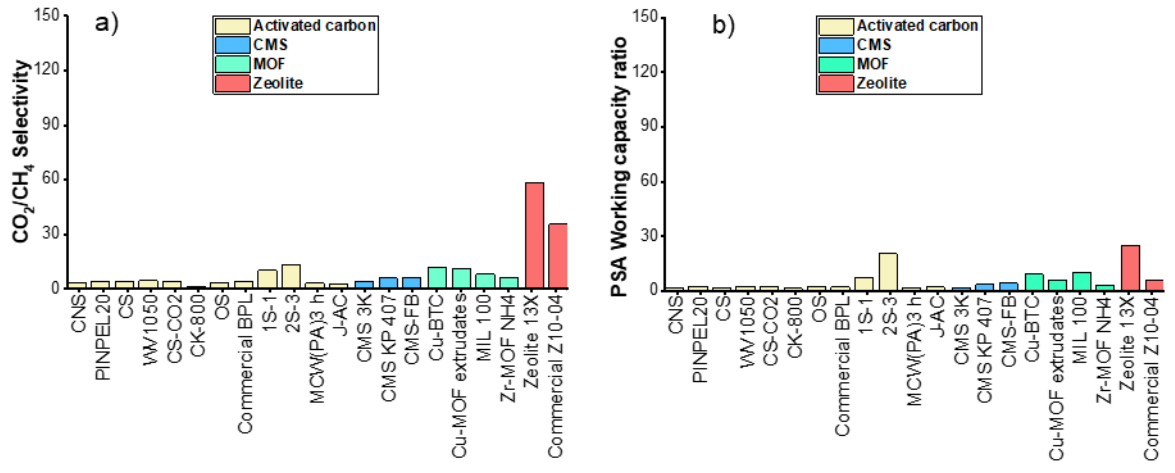
1500 equalization; *PPE*: pressurization pressure equalization; *IDEL*: standby.

1501

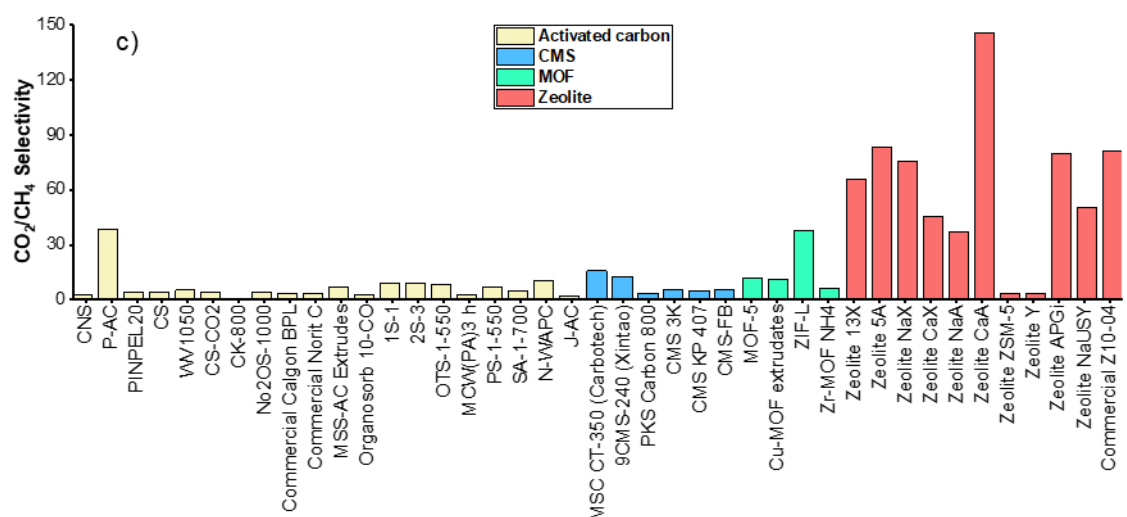
1502

1503

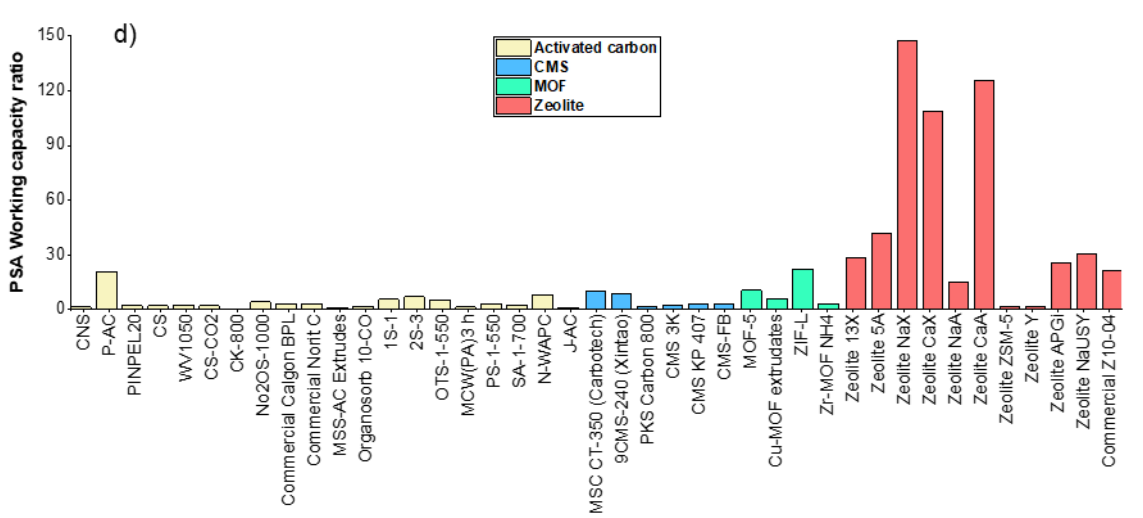
1504



1505



1506



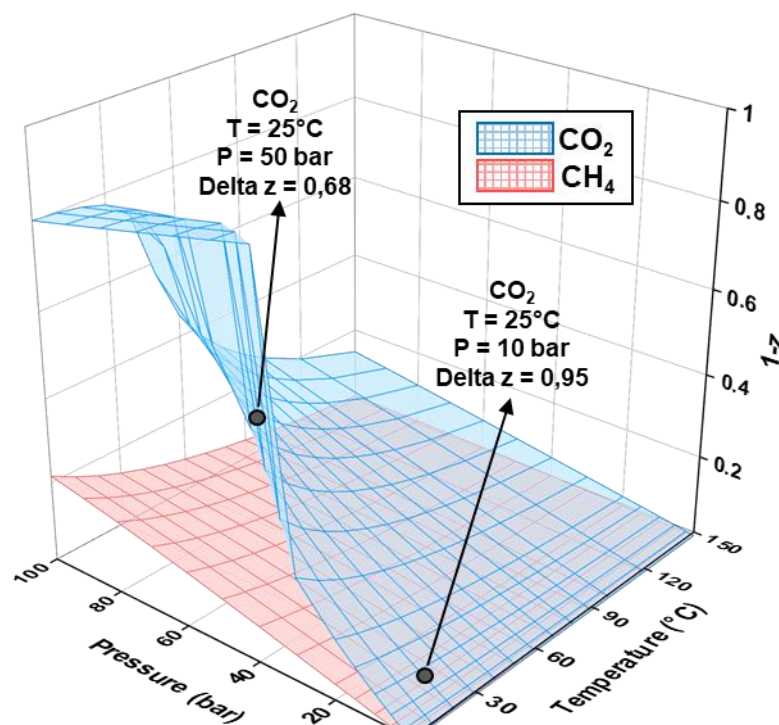
1507

1508 **Figure 5.** Comparison of CO<sub>2</sub>/CH<sub>4</sub> equilibrium selectivity and PSA working capacity  
 1509 ratio for various adsorbents at a gas composition of CO<sub>2</sub> = vol. 35% and CH<sub>4</sub> = vol.  
 1510 65%. a) Selectivity at 5 bar, b) PSA working capacity ratio at:  $P_a = 5$  bar,  $P_d = 1$  bar. c)

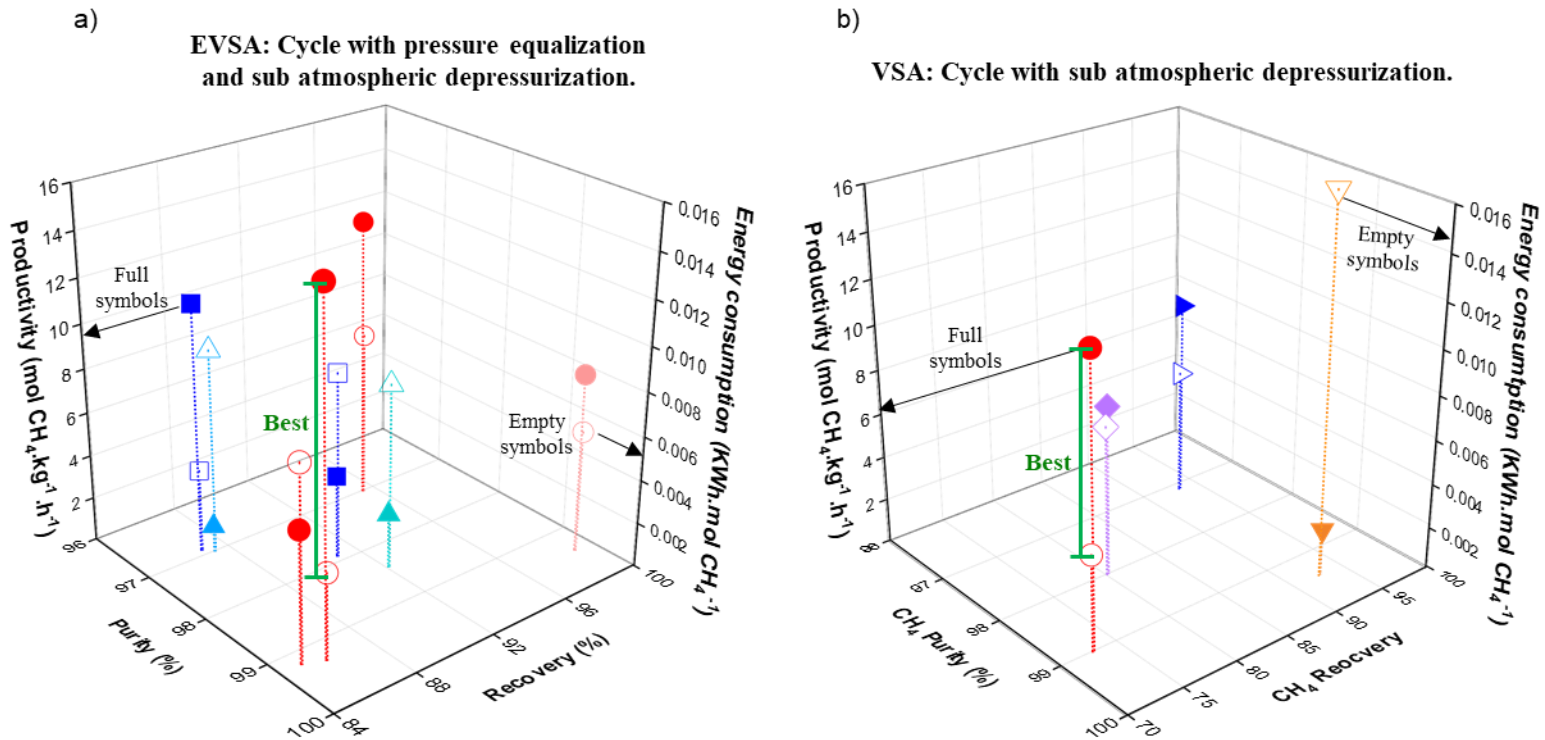


1511 Selectivity at 1 bar, d) PSA working capacity ratio at:  $P_a = 1$  bar,  $P_d = 0.2$  bar. – CNS<sup>[44]</sup>, P-  
 1512 AC, PINPEL20<sup>[45]</sup>, CS<sup>[37]</sup>, Commercial WV1050<sup>[37]</sup>, CS-CO2<sup>[36]</sup>, CK-800<sup>[49]</sup>, OS<sup>[123]</sup>, No2OS-1000<sup>[124]</sup>,  
 1513 Commercial calgon BPL<sup>[124]</sup>, Commercial Norit C<sup>[124]</sup>, MSS-AC Extrudates<sup>[48]</sup>, Organosorb 10-CO<sup>[77]</sup>, 1S-1<sup>[42]</sup>,  
 1514 2S-3<sup>[42]</sup>, OTS-1-550<sup>[3]</sup>, MCW(PA)3h<sup>[46]</sup>, PS-1-550<sup>[125]</sup>, SA-1-700<sup>[51]</sup>, N-WAPC<sup>[53]</sup>, J-AC<sup>[52]</sup>, MSC CT-  
 1515 350(Carbotech)<sup>[77]</sup>, CMS-240(Xintao)<sup>[77]</sup>, PKS Carbon 800<sup>[126]</sup>, CMS-3K<sup>[107]</sup>, CMS KP 407<sup>[127]</sup>, CMS-FB<sup>[128]</sup>,  
 1516 MOF-5<sup>[76]</sup>, Cu-BTC<sup>[61]</sup>, Cu-MOF extrudates<sup>[129]</sup>, MIL100<sup>[130]</sup>, ZIF-L<sup>[131]</sup>, Zr-MOF NH4<sup>[132]</sup>, Zeolite 13X<sup>[61]</sup>,  
 1517 Zeolite 5A<sup>[76]</sup>, Zeolite NaX<sup>[78]</sup>, Zeolite CaX<sup>[78]</sup>, Zeolite NaA<sup>[78]</sup>, Zeolite CaA<sup>[78]</sup>, Commercial Z10-04<sup>[79]</sup>. Note  
 1518 that zeolites NaX and 13X are the same, as are zeolites 5A and CaA, but we have left the original names  
 1519 as given in the bibliographical sources, these sources giving slightly different results, as shown in the  
 1520 graphs.

1521  
 1522  
 1523



1524  
 1525 **Figure 6.** 1-z (1-Compressibility factor) for CO<sub>2</sub> and CH<sub>4</sub> as a function of temperature  
 1526 and pressure.  
 1527



1528

1529 **Figure 7.** Purity, recovery, productivity and energy consumption plots for CO<sub>2</sub>/CH<sub>4</sub>  
 1530 separation by EVSA and VSA: a) EVSA cycle, b) VSA cycle – Full symbols represent  
 1531 productivity and empty symbols represent energy consumption - ●: 2-bed Zeolite<sup>[39, 59,</sup>  
 1532 <sup>75, 79]</sup> - ■: 2-bed CMS<sup>[79, 111]</sup> - ▲: 3-bed + 1tank CMS<sup>[112]</sup> - ▲: 5-bed CMS<sup>[93]</sup> - ●: 4-bed  
 1533 Zeolite<sup>[115]</sup> - ◆: 2-bed Zeolite + CMS<sup>[38]</sup> - ▼: 4-bed MOF + CO<sub>2</sub> production.<sup>[68]</sup> - ►:  
 1534 6-bed CMS<sup>[114]</sup> - | Best PSA-adsorbent configuration.